Answers Research Journal 3 (2010):165–190.
www.answersingenesis.org/arj/v3/geology-israel-pre-flood.pdf

The Geology of Israel within the Biblical Creation-Flood Framework of History: 1. The pre-Flood Rocks

Andrew A. Snelling, Answers in Genesis, P.O. Box 510, Hebron, Kentucky 41048

Abstract

Precambrian (pre-Flood) schists, gneisses, and related metamorphic rocks, intruded by granites outcrop in the Elat area of southern Israel. Their radioisotope ages range from 800–813 Ma to 600 Ma. Also, just to the north of Elat is the Timna Igneous Complex, a 610–625 Ma series of granitic intrusions. All these rock units across this region were then intruded along fractures by swarms of dikes. Together these metamorphic and igneous rocks form the northernmost part of the Arabian-Nubian Shield, which would have likely been a section of the pre-Flood supercontinent Rodinia, established by God's creative activity on Day Three of the Creation Week. It is thus envisaged that this cataclysmic rate of formation of these rocks during an episode of accelerated radioisotope decay accounts for their apparent long history when wrongly viewed in the context of today's slow process rates. Unconformably overlying these Precambrian crystalline basement rocks are terminal Precambrian conglomerates, arkoses, and interbedded, explosively-erupted volcanics that were obviously deposited by catastrophic debris avalanches as the pre-Flood supercontinent began to break up, with accompanying igneous activity that coincided with the bursting forth of the fountains of the great deep. It is envisaged that another episode of accelerated radioisotope decay must have begun months previously, the released heat progressively increasing so as to initiate the igneous activity that ultimately triggered the renting apart of the pre-Flood supercontinent at the onset of the Flood cataclysm. The pre-Flood/Flood boundary in southern Israel is thus determined as the major unconformity between the Precambrian crystalline basement and the overlying terminal Precambrian conglomerates, arkoses and volcanics, almost identical to that boundary as determined in the U.S. Southwest. The few ^{210}Po radiohalos found in some of the basement granitic rocks are likely due to the basinal fluids that flowed from the basal Flood sediments when heated by burial under the overlying thick, rapidly-accumulated sequence of Flood sediments.

Keywords: Israel, geology, pre-Flood, Precambrian, schists, gneisses, granites, dikes, radioisotope ages, radiohalos, Arabian-Nubian Shield, conglomerates, volcanics, accelerated radioisotope decay, unconformity, pre-Flood/Flood boundary

Introduction

Of the many countries whose geology would be useful to understand within the biblical creation-Flood framework of earth history it would be Israel. Israel is the land in which so many post-Flood biblical events occurred. Understanding the geology of Israel would thus provide background to those biblical events, and potential insights as to where and how they happened. However, there is also the possibility some of the early post-Flood biblical events may correspond to geologic events responsible for specific rock formations, and therefore date those rock layers within the biblical chronology.

The land of Israel certainly did not exist in its present form prior to the Flood, which totally restructured and re-shaped the earth's crust and surface. For example, the Dead Sea trough and Jordan River valley lie along a major north-south fault zone, a narrow system of faults called the Dead Sea Transform Fault, which is the primary geologic structure in Israel (fig 1). This fault system extends today from the major fold mountains of southern Turkey southward through Syria, Lebanon, Jordan, Israel, and the Gulf of Aqaba to the zone of pronounced rift faulting in the Red Sea and beyond into Africa. The Dead Sea Transform Fault marks the boundary between two enormous lithospheric plates, the Arabian plate to the east, and the African plate to the west (fig. 1). Rock types and geologic structures on both sides of this enormous horizontal-slip fault suggest that the Arabian plate has moved northward horizontally by about 95 km (60 miles) relative to its original position against the African plate.

It is because of this and other dramatic evidence of major movements of the earth's lithospheric plates in the past having shaped the earth's surface geology, composed in many places on the continents of fossil-bearing sedimentary rock layers which were deposited by the Flood, that the Flood must have been a global tectonic catastrophe. Therefore, the model for the Flood event adopted here is catastrophic plate tectonics (Austin et al. 1994; Baumgardner 2003). A fuller treatment of the application of that model to the geologic record within the biblical creation-Flood

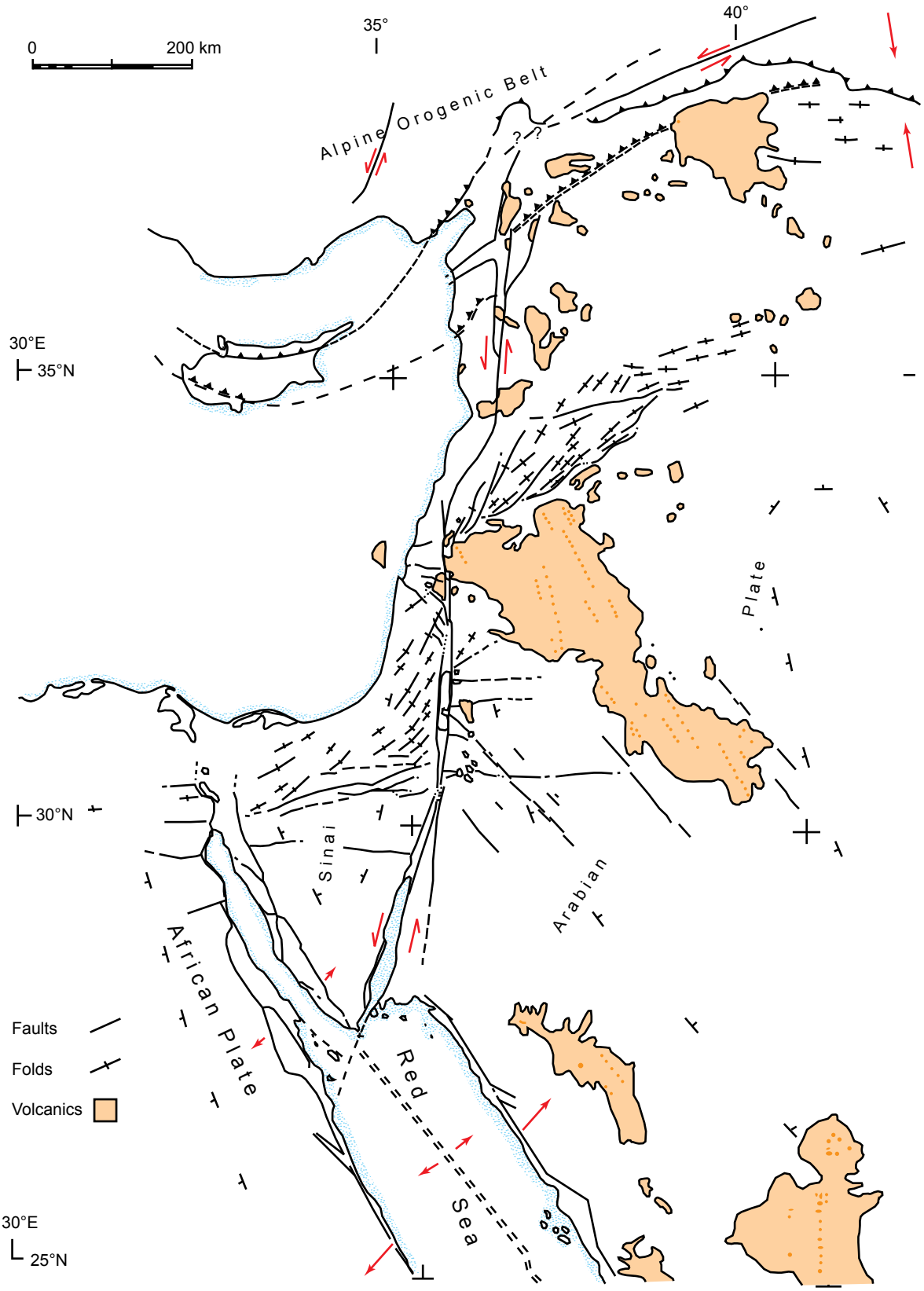

Fig. 1. Geologic structure map of Israel and its adjoining neighbors showing major faults and folds (after Garfunkel 1978).

framework of earth history is provided by Snelling (2009). That treatment also includes discussion of the criteria for determining the pre-Flood/Flood boundary in the geologic record, which is also applicable to the descriptive overview here of the pre-Flood geology of Israel.

Pre-Flood Rock Units

Fig. 2 is a fairly detailed map of the geology of the southern half of Israel (Sneh et al. 1998) where pre-Flood rocks outcrop. Fig. 3 is a generalized stratigraphic chart showing the succession of rock units across Israel (Bartov and Arkin 1980; Ilani, Flexer, and Kronfeld 1987). The only Precambrian crystalline basement rocks at the base of the stratigraphic succession are in the extreme south of Israel, around Elat. A more detailed geological map of that area is shown in Fig. 4.

These pre-Flood crystalline basement rocks consist of granitic and metamorphic rocks. Garfunkel (1980) provides a comprehensive description of these rocks, dividing them into the Elat and Roded associations (or terrains), and the Timna Igneous Complex (table 1).

The Elat Association (or Terrain)

Just to the south and west of Elat (fig. 4) outcrops consist of Elat Schist, the Taba Gneiss, the Shahmon Metabasites, the Elat Granite Gneiss, and the Elat Granite (Garfunkel 1980; Halpern and Tristan 1981; Kröner, Eyal and Eyal 1990) (table 1). The relationships between these rock units are depicted in the cross-section in Fig. 5.

The Elat Schist has been determined stratigraphically as the oldest rock unit, which has been confirmed by an Rb-Sr isochron age determination of 807±35 Ma (Halpern and Tristan 1981), and by zircon U-Pb age determinations of 800±13 Ma and 813±7 Ma (Eyal, Eyal, and Kroner 1991; Kröner, Eyal and Eyal 1990). It is a monotonous formation which consists primarily of a mosaic of quartz, plagioclase (oligoclase-andesine), biotite, and some muscovite in variable proportions, with minor intercalations of impure quartzitic layers up to 10 cm thick. Mineralogical and geochemical data support a pelitic or shaly-graywacke (semipelitic) origin for most of this unit (Eyal 1980), which is estimated to be 5–10 km thick normal to the strike of the schistosity, and which has experienced prograde regional metamorphism well into the amphibolite facies, but of the low pressure (Abukuma) type, similar to other parts of the Arabian-Nubian Shield (Shimron and Zwart 1970). The lowest grade rocks, within the biotite isograd, occur in the north and are biotite-muscovite-chlorite garnet-bearing schists. Most of the Elat Schist consists of rocks within the garnet (almandine) isograd and does not contain primary chlorite. A small area is within the staurolite isograd, while cordierite occurs in even smaller areas. Andalusite occurs in the latter two zones, while primary muscovite is uncommon, in contrast to the lower grade rocks. The cordierite-staurolite assemblage of the highest grade rocks indicates maximum temperatures in the range of 550–650°C, and pressures of 2–5 kbar, equivalent to a depth of about 7–15 km (Ganguly 1972; Winkler 1979). Mineral analyses have been used by Matthews et al. (1989) to calculate, on the basis of continuous reaction exchange geothermobarometry (Mg/Fe between garnet and biotite; Ca between garnet and plagioclase), that conditions for a segment of the pressure-temperature path of the high grade staurolite-cordierite-sillimanite zone assemblages were 580–600°C and 3.8–4.6 kbar. The schists bear evidence of four stages of mineral growth and deformation. The Elat Schist was intruded by a variety of plutonic rock units, now mostly gabbroic to granitic orthogneisses, the most prominent being the Taba Gneiss and the Elat Granite Gneiss.

The Taba Gneiss is a foliated and lineated, medium-grained quartz-diorite gneiss (fig. 4 and table 1), consisting of quartz (25%), plagioclase (oligoclase) (50–60%), and biotite, rarely with some hornblende or microcline (Garfunkel 1980; Halpern and Tristan 1981). The rock is usually uniform, but occasionally has an indistinct coarse layering. Contacts with the schists are sharp. Its texture is dominated by elongated aggregates of the main constituent minerals, which produce the pronounced lineation and moderate to weak foliation. Grain sizes are very variable. The texture seems to indicate formation from a coarse-grained tonalitic pluton, followed by metamorphism and incomplete post-deformational recrystallization. To the west of Elat this gneiss is intensely deformed in a broad shear zone so the rock has a schistose appearance and has been mapped as a "tectonic schist" (Kröner, Eyal, and Eyal 1990). Ages have been determined by zircon U-Pb analyses at 780±10 Ma and 770±9 Ma for this gneiss and this schist respectively (Kröner, Eyal, and Eyal 1990), and of 779±8 Ma and 782±9 Ma for the gneiss and 768±9 Ma for the schist (Eyal, Eyal, and Kröner 1991). These ages are indistinguishable within the error margins, so this confirms the field interpretation that the tectonic schist represents a strongly sheared variety of the Taba Gneiss.

The Elat Granite Gneiss was formed from granitic plutons emplaced into the pelitic Elat Schist and the Taba Gneiss, and also from small tabular bodies emplaced in the Taba Gneiss (Garfunkel 1980; Halpern and Tristen 1981). It is composed of about equal amounts of quartz, plagioclase (oligoclase) and alkali feldspar, with biotite accounting for 5–15% of the rock. The main minerals, especially quartz

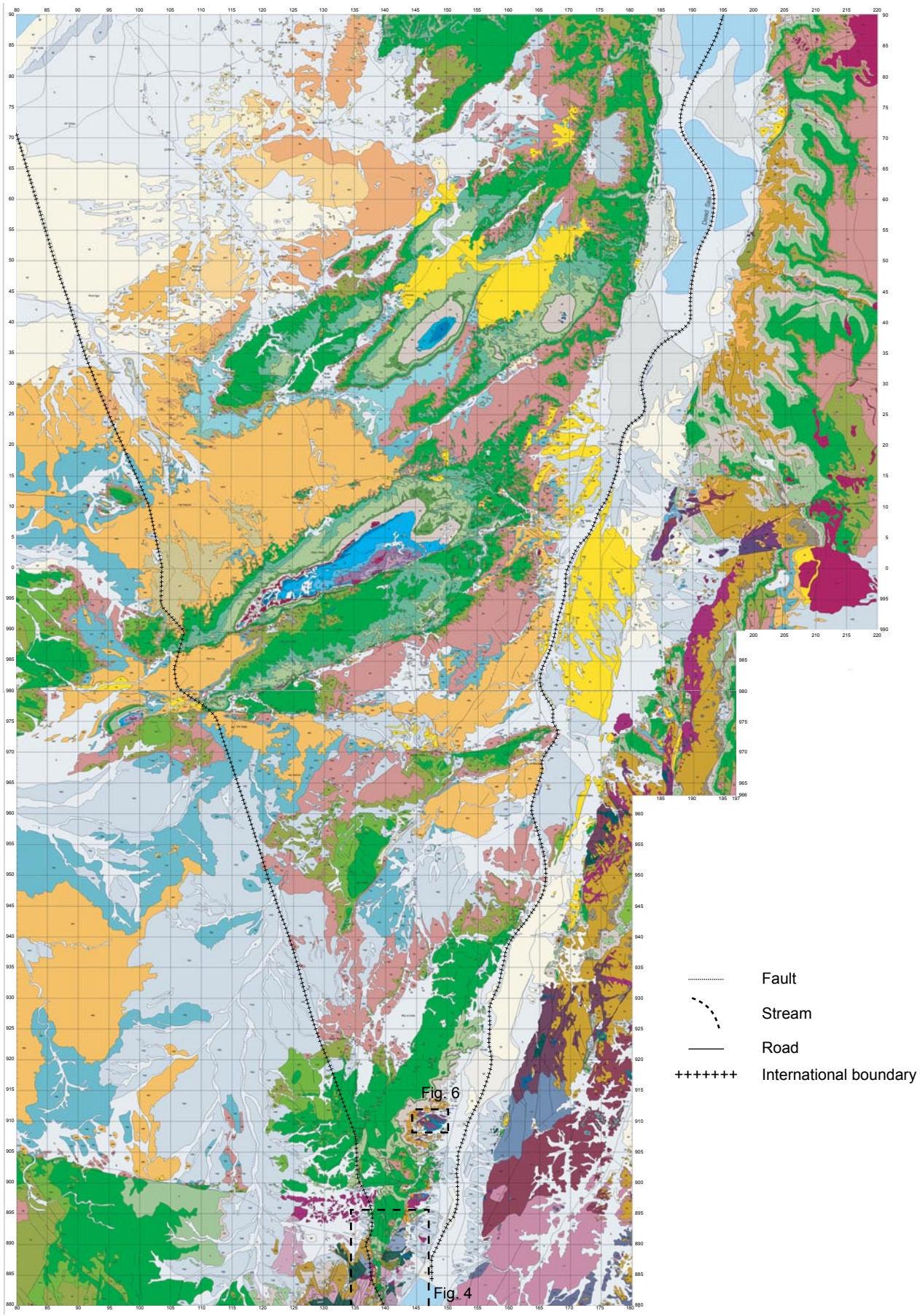
Fig. 6
Fig. 4
Fault
Stream
Road
International boundary

Symbol	Area	Geology
t	Northern Negev	**Bina Formation Derorim, Shivta and Nezer Formations, Ora and Gerofit Formations, Shuay'b and Wadi as Sir Formations*** (Limestone, dolostone, conglomerate, sandstone 172 m) *Turonian*
t	Negev	**Ore and Gerofit Formations, Shay'b and Wadi as Sir Formations (Jordan)** (Marl, limestone, sandstone 276 m) *Turonian*
c	Central	**Albian-Cenomanian (Jordan)** (Limestone, dolostone, chalk, marl) *Turonian*
c	Northern Negev	**Hazera Formation in Sinari Naur, Fuheis and Hummar Formations (Jordan)** (Limestone, dolostone, chalk, marl) *Albian-Cenomanian*
c	Negev	**Hazera Formation in Sinari Naur, Fuheis and Hummar Formations (Jordan)** (Limestone, dolostone, chalk, marl) *Albian-Cenomanian*
c3	North	**Sakhnin and Yanuh Formations** (Dolostone, limestone, chert 205 m) *Cenomanian*
c3	Central	**Weradim Formation, Tamar Formation** (Dolostone 160 m) *Cenomanian*
c3	Northern Negev	**Weradim Formation, Tamar Formation** (Dolostone, limestone, chert 58 m) *Cenomanian*
c3	Negev	**Tamar Formation** (Dolostone 31 m) *Cenomanian*
c2	North	**Deir Hanna Formation, Isfiya Chalk, Bet Oren Limestone, Khuriebe Chalk and Junediya Chalk** (Limestone, dolostone, marl, chalk, chert 330 m) *Cenomanian*
c2	Central	**Bet Meir, Moza, Amminadav and Kefar Shaul Formations, En Yorqe'am, Zafit and Avnon Formations** (Limestone, dolostone, marl) *Cenomanian*
c2	Northern Negev	**En Yorqe'am, Zafit and Avnon Formations, Bet Meir, Moza, Amminadav and Kefar Shaul Formations** (Limestone, dolostone, marl, chalk, chert 210 m) *Cenomanian*
c2	Negev	**En Yorqe'am, Zafit and Avnon Formations** (Limestone, dolostone, chalk, marl, chert 124 m) *Cenomanian*
c1	North	**Yagur Formation, Kammon Formation** (Dolostone 197 m) *Albian-Cenomanian*
c1	Central	**Givat Ye'arim, Soreq and Kesalon Formations, Hevyon Formation** (Limestone, dolostone, marl, chalk, chert 227 m) *Albian-Cenomanian*
c1	Northern Negev	**Hevyon Formation, Givat Ye'arim, Soreq and Kesalon Formations** (Limestone, dolostone, marl, chalk, chert 160 m) *Albian-Cenomanian*
c1	Negev	**Hevyon Formation** (Limestone, dolostone, marl, chert, sandstone 44 m) *Albian-Cenomanian*
lc	North	**Nabi Sa'id, Ein el Assad, Ildra, Rama and Kefira Formations** (Limestone, chalk, marl, sandstone 430 m) *Lower Cretaceous*
lc	Central	**Nabi Sa'id, Ein el Assad, Ildra, Rama and Kefira Formations** (Limestone, marl, chalk, sandstone 670 m) *Lower Cretaceous*
lck	North	**Kurnub Group** (Sandstone 85 m) *Lower Cretaceous*
lck	Central	**Kurnub Group** (Sandstone, clay, limestone 120 m) *Lower Cretaceous*
lck	Northern Negev	**Kurnub Group** (Sandstone, pebbly sandstone, marl, mudstone, clay, limestone, dolostone, conglomerate 408 m) *Lower Cretaceous*
lck	Negev	**Kurnub Group** (Sandstone, mudstone, clay, pebbly sandstone, conglomerate 240 m) *Lower Cretaceous*
im	North	**Intrusions and volcaniclastic rocks** (Diabase, microgabbro) *Mesozoic*
im	Northern Negev	**Intrusions rocks** (Andesite and trachite dykes, syenite quartz syenite, gabbro) *Mesozoic*
im	Negev	**Intrusions and volcaniclastic rocks** (Basalt) *Mesozoic*
βlc	North	**Basalt flows** (Basalt, basanite) *Lower Cretaceous*
βlc	Central	**Tayasir Volcanics** (Basalt/flows and volcaniclastics) *Lower Cretaceous*
βlc	North Negev	**Basalt flows and volcaniclastics** (Basalt, basanite, tephrite, nephelinite) *Lower Cretaceous*
βlc	Negev	**Basalt flows** (Basalt, basanite, tephrite, nephelinite) *Lower Cretaceous*
ju	General	**Upper Jurassic** (Limestone 193 m) *Lower Cretaceous*
ju2	North	**Be'er Sheva and Haluza Formations** (Limestone, marl 85 m) *Upper Jurassic*
ju2	Northern Negev	**Be'er Sheva and Haluza Formations** (Limestone, marl 100 m) *Upper Jurassic*
ju1	Northern Negev	**Kidod Formation** (Clay, limestone, dolostone 155 m) *Upper Jurassic*
ju1	North	**Kidod Formation** (Clay, limestone, dolostone 30 m) *Upper Jurassic*
jm	Central	**Hermon Formation** (Limestone, dolostone 623 m) *Middle Jurassic*
jm	Northern Negev	**Middle Jurassic (Jordan)** (Limestone, marl 76 m) *Middle Jurassic*
jm	Northern Negev	**Mahmal, Zohar and Matmor Formations** (Sandstone, limestone, marl, clay) *Middle Jurassic*
jl2	Negev	**Inmar Formation** (Sandstone, clay 340 m) *Lower Jurassic*
jl2	Northern Negev	**Inmar Formation** (Sandstone, clay 120 m) *Lower Jurassic*
jl1	Negev	**Mishhor and Ardon Formations** (Dolostone, limestone, clay, sandstone 70 m) *Lower Jurassic*
jl1	Central	**Mishhor and Ardon Formations** (Dolostone, limestone, clay, sandstone 21 m) *Lower Jurassic*
trs	Northern Negev	**Upper Triassic (Jordan)** (Sandstone, limestone, clay, gypsum) *Lower Jurassic*
trs	Northern Negev	**Mohilla Formation** (Gypsum, dolostone, limestone, clay 202 m) *Upper Triassic*
tr2	Negev	**Saharonim Formation** (Limestone, clay, marl, dolostone, sandstone, gypsum 174 m) *Middle Triassic*
tr2	Northern Negev	**Saharonim Formation** (Limestone, clay, marl, dolostone, sandstone, gypsum 117 m) *Middle Triassic*
tr1	Negev	**Gevanim Formation** (Siltstone, clay, quarzite, sandstone, limestone, gypsum +166 m) *Lower Triassic*
tr1	General	**Gevanim Formation** (Sandstone, limestone, siltstone, clay 68 m) *Lower Triassic*
tr1r	General	**Ra'af Formation** (Dolostone, marl, limestone +32 m) *Lower Triassic*
tr	Northern Negev	**Permian and Triassic (Jordan)** (Sandstone, siltstone, mudstone) *Lower Triassic*
or	Negev	**Disi Sandstone Formation (Jordan)** (Sandstone, siltstone, mudstone) *Ordovician*
or	Central	**Disi Sandstone Formation (Jordan)** (Sandstone, pebbly sandstone, siltstone) *Ordovician*
cb	Northern Negev	**Umm Ishrin Sandstone Formation (Jordan)** (Sandstone, mudstone) *Cambrian*
cb	Negev	**Umm Ishrin Sandstone Formation, with Salib Formation where Burj Formation absent (Jordan)** (Sandstone, mudstone) *Cambrian*
cb	General	**Umm Ishrin Sandstone Formation, with Salib Arkosic Sandstone Formation where Burj Dolomite-Shale Formation absent* (Jordan)** (Sandstone, mudstone) *Cambrian*
cb2	General	**Shehoret and Netafim Formations** (Pebbly sandstone, sandstone, dolostone, limestone, siltstone, mudstone, conglomerate 165 m) *Cambrian*
cb1	Central	**Amudei Shelomo and Timna Formations** (Pebbly sandstone, sandstone, conglomerate, mudstone, dolostone, limestone 135 m) *Cambrian*
cbb	Northern Negev	**Burj Dolomite-Shale Formation (Jordan)** (Sandstone, dolostone, mudstone) *Cambrian*
cbb	General	**Salih Arkosic Sandstone Formation and Burj Dolomite-Shale Formation (Jordan)** (Sandstone, dolostone, mudstone) *Cambrian*
cby	General	**Yam Suf Group** (Sandstone, pebbly sandstone, conglomerate, mudstone, dolostone, limestone) *Cambrian*
πC	General	**Elat Conglomerate, Roded Conglomerate** (Sandstone, pebbly sandstone, conglomerate, mudstone, dolostone, limestone) *Precambrian*
γt	General	**Timna Granite, Shahmon Granite, Yehoshafat Granite, Amram Granite Porphyry** (Sandstone, pebbly sandstone, conglomerate, mudstone, dolostone, limestone) *Precambrian*
γ	General	**Elat Granite, Roded Granite Porphyry, Timna Granite Porphyry** (Sandstone, pebbly sandstone, conglomerate, mudstone, dolostone, limestone) *Precambrian*
σ	General	**Syenite, Monzonite and other intermediate rocks** (Sandstone, pebbly sandstone, conglomerate, mudstone, dolostone, limestone) *Precambrian*
δ	General	**Gabbro, diorite, and other basic rocks** (Sandstone, pebbly sandstone, conglomerate, mudstone, dolostone, limestone) *Precambrian*
qδr	General	**Roded Quartz-Diorite** (Sandstone, pebbly sandstone, conglomerate, mudstone, dolostone, limestone) *Precambrian*
α	General	**Amphibolite** (Sandstone, pebbly sandstone, conglomerate, mudstone, dolostone, limestone) *Precambrian*
γγv	General	**Granitic Gneiss** (Sandstone, pebbly sandstone, conglomerate, mudstone, dolostone, limestone) *Precambrian*
γv	General	**Taba Gneiss** (Sandstone, pebbly sandstone, conglomerate, mudstone, dolostone, limestone) *Precambrian*
μι	General	**Roded and Elat Schist, Gneiss and Migmatite** (Sandstone, pebbly sandstone, conglomerate, mudstone, dolostone, limestone) *Precambrian*
va	General	**Ahaymir Volcanics (Jordan)** (Sandstone, pebbly sandstone, conglomerate, mudstone, dolostone, limestone) *Precambrian*
pem	General	**Muffaraqad Conglomerate (Jordan)** (Sandstone, pebbly sandstone, conglomerate, mudstone, dolostone, limestone) *Precambrian*
γf	General	**Finan Granite (Jordan)** (Sandstone, pebbly sandstone, conglomerate, mudstone, dolostone, limestone) *Precambrian*
δq	General	**Qunai Diorite (Jordan)** (Sandstone, pebbly sandstone, conglomerate, mudstone, dolostone, limestone) *Precambrian*
pes	General	**Saramuj Conglomerate Formation (including Hayall Formation)** (Sandstone, pebbly sandstone, conglomerate, mudstone, dolostone, limestone) *Precambrian*
γs	General	**Sammaniya Microgranite** (Sandstone, pebbly sandstone, conglomerate, mudstone, dolostone, limestone) *Precambrian*
γy	General	**Yutum Granite** (Sandstone, pebbly sandstone, conglomerate, mudstone, dolostone, limestone) *Precambrian*
μm	General	**Minshar Monzogranite (Jordan)** (Sandstone, pebbly sandstone, conglomerate, mudstone, dolostone, limestone) *Precambrian*
vg	General	**Ghuwayr Volcanics (Jordan)** (Sandstone, pebbly sandstone, conglomerate, mudstone, dolostone, limestone) *Precambrian*
πu	General	**Urf Porphyry (Jordan)** (Sandstone, pebbly sandstone, conglomerate, mudstone, dolostone, limestone) *Precambrian*
γth	General	**Thaur Gabbro** (Sandstone, pebbly sandstone, conglomerate, mudstone, dolostone, limestone) *Precambrian*
δr	General	**Rachel Hornblende Quartz-Diorite** (Sandstone, pebbly sandstone, conglomerate, mudstone, dolostone, limestone) *Precambrian*
γδr	General	**Rumman Granodiorite** (Sandstone, pebbly sandstone, conglomerate, mudstone, dolostone, limestone) *Precambrian*
τd	General	**Darba Tonalitic** (Sandstone, pebbly sandstone, conglomerate, mudstone, dolostone, limestone) *Precambrian*
μr	General	**Rahma Foliated Granitoid (Jordan)** (Sandstone, pebbly sandstone, conglomerate, mudstone, dolostone, limestone) *Precambrian*
μj	General	**Janub Metamorphics** (Sandstone, pebbly sandstone, conglomerate, mudstone, dolostone, limestone) *Precambrian*
μs	Negev	**Abu Saqa'a Schist** (Chalk, chert 105 m) *Precambrian*
μh	Negev	**Duhayla Hornblendite** (Chalk, chert 105 m) *Precambrian*
γγb	General	**Abu Barqa Metasediments Buseinat Gneiss** (Sandstone, pebbly sandstone, conglomerate, mudstone, dolostone, limestone) *Precambrian*

Fig. 2. Detailed geologic map of the southern half of Israel, from the Dead Sea to Elat on the Red Sea and encompassing the Negev (left) (after Sneh et al. 1998). The only Precambrian (pre-Flood) rocks are found in the outlined areas enlarged in Figs. 4 and 6. Details of most of the rock units on the map are listed in the legend.

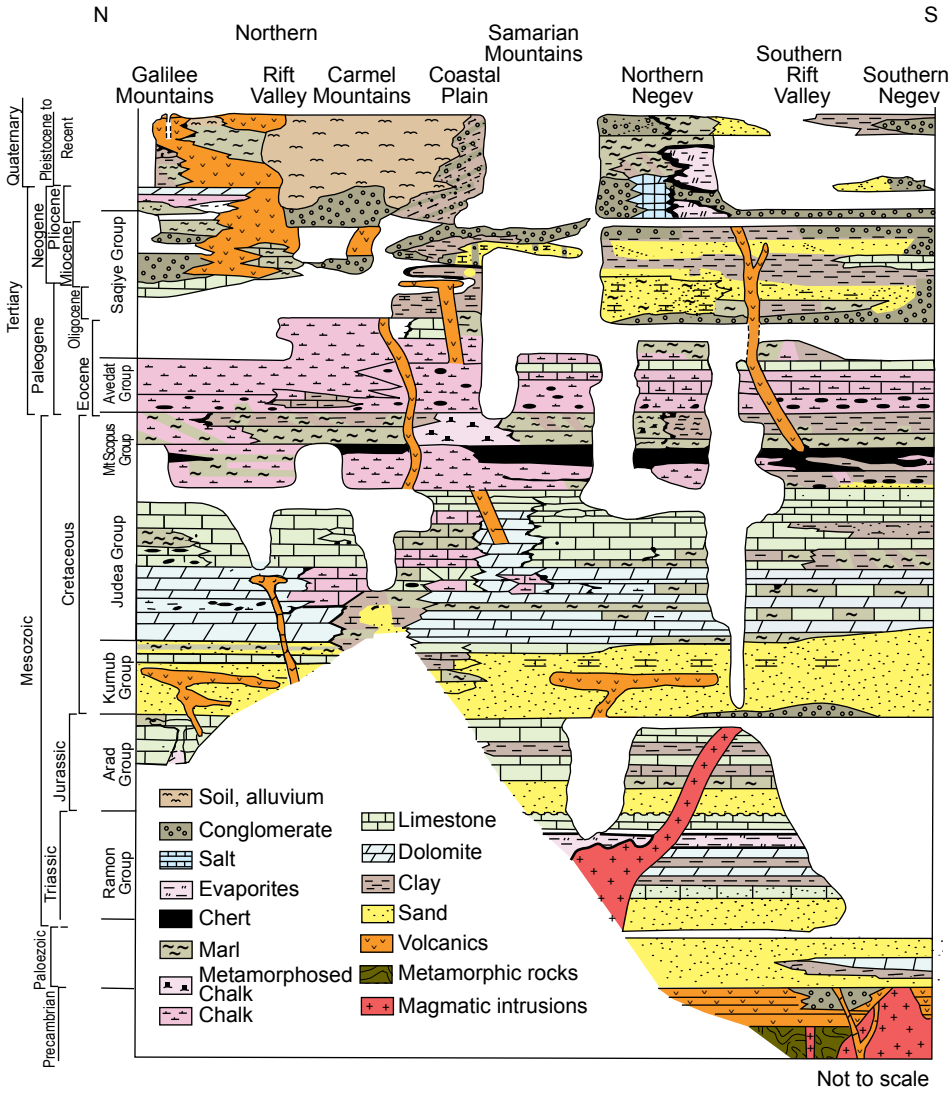

Fig. 3. A generalized stratigraphic chart showing the succession of rock units (their names and geologic ages) across Israel from south (right) to north (left) (after Bartov and Arkin 1980; Ilani et al. 1987).

and biotite, tend to form elongated aggregates. The texture is very variable and displays varying grades of recrystallization due to deformation (Heinmann et al. 1995). The contacts with the surrounding rocks are generally concordant, and often accompanied by feldspathization of the adjacent rocks. This aureole, and the occurrence in places of schist xenoliths, indicates that the original granite was emplaced into already metamorphosed Elat Schist. Foliation and lineation vary from indistinct to very prominent, but lineations are generally better developed. Both the lineations and foliations of the gneiss are parallel to the contacts and to structures in the enclosing rocks. Single grain zircon U-Pb determinations yield a mean $^{207}Pb/^{206}Pb$ age of 744±5 Ma, slightly younger than the Taba Gneiss and thus confirming the field relationships.

The Shahmon Metabasites intrude the Elat Schist and comprise a suite of coarse- to medium-grained metamorphosed plutonic rocks that originally consisted of a layered and differentiated intrusion a few hundred meters thick. They form a diverse range of compositions, from hornblende metagabbro to biotite hornblende metadiorite (Heinmann et al. 1995), but commonly consist of plagioclase (andesine-labradorite) and amphiboles. Variations in the amounts of these minerals and in grain size produce bands and layers less than 1 cm to many meters thick. A border zone consists of well-layered rocks having a biotite- and quartz-dioritic composition, and near the borders the metabasites contain interbeds of schist. This banding, layering and border facies are interpreted as a result of crystal accumulation and gross differentiation of the original intrusion. The occurrence of actinolite and plagioclase, but no epidote, in these rocks indicates metamorphism of them reached low amphibolite facies, which is compatible with their position close to the almandine isograd

in the surrounding schists. Foliation and mineral orientation are poorly or moderately developed, except in the mica-rich layers and in the border zone where the structure is concordant with that of the enclosing schists. Originally thought to be the oldest plutonic assemblage of the area with primary igneous layering well preserved, abundant elongated xenoliths of foliated Elat Schist indicate that the diorite-gabbro intrusion post dated at least part of the schist deformation. This is confirmed by single-grain zircon U-Pb age determinations of 640±12 to 644±11Ma (Kröner, Eyal, and Eyal 1990), and of 640±10Ma (Eyal, Eyal, and Kröner 1991). Amphiboles from this metabasite also yielded a mean Ar-Ar plateau age of 632Ma (Heimann et al. 1995) and an imprecise Ar-Ar isochron age of 625±88Ma (due to the presence of excess Ar) (Cosca, Shimron, and Caby 1999). These age determinations are thus consistent with the field evidence that this suite of mafic plutonic rocks intrudes and crosscuts the foliation of the older host Elat Schist, even though these metabasites show varying degrees of deformation and recystallization that occurred subsequent to their intrusion.

Straight and rather steeply-dipping bands of lineated hornblende-bearing schistose rocks cross all rock types already described above. They are up to a few meters wide and a few hundred meters long, strike E-W to NE-SW, and tend to form swarms. Bentor (1961) interpreted these bands as metamorphosed dikes. They consist now of plagioclase (andesine) (up to 60%), biotite (20–30%), and hornblende (10–20%), with quartz minor or absent, and sphene, apatite and iron oxides as usual accessories. This mineralogy indicates metamorphism in the low amphibolite facies, which is generally not much different from the grade of the enclosing pelitic schists. Cohen et al. (2000) and Katz et al. (2004) determined that the original chemical composition of these dikes was andesite, which was little changed by this metamorphism, except where hot fluids had caused minor alteration, mainly along the contacts with the host rocks. The texture consists of a granoblastic mosaic, with the mafic minerals arranged in layers or sheaves. Grain size is uniform. Lineation is very well developed and mostly parallel to that in the enclosing rocks. Good foliation is sometimes developed. The fabrics are conspicuously parallel to the walls of the dikes, but sometimes are deformed and deviate by up to 20°–30° from the walls. These relationships indicate that the dikes were intruded after the development of the schistosity, and after folding of the contact with the granitic gneiss. Subsequently a penetrative lineation was imposed on all rocks. This lineation was clearly produced during metamorphism of the dikes, and is thus younger than the foliation of the pelitic schists. This late deformation was inhomogeneous, being very strong in the dikes themselves, and often also in the adjacent granitic gneiss, but mild in the pelitic schists even immediately adjacent to the dikes where the older schistosity survived. Heimann et al. (1995) obtained $^{40}Ar/^{39}Ar$ total-gas ages of 495–592Ma for amphiboles and 446Ma and 316–336Ma (average 327Ma) for biotites, compared with $^{40}Ar/^{39}Ar$ plateau ages of 546±3Ma to 596±2Ma (amphiboles) and 369±2Ma to 389±1Ma (biotites). Such a broad range of ages was interpreted as implying two thermal events affecting these dikes subsequent to their intrusion—the first coinciding with intrusion of the Elat Granite (recorded by the amphiboles), and a much later thermal event (recorded by the biotites). However, there are two generations of these metamorphosed andesite dikes in the Roded area, one which is discordant to the metamorphic structure of the country rocks and which intrudes the Roded Quartz-Diorite, and the other which is concordant to the metamorphic structure but which does not intrude the Roded Quartz-Diorite (Katz et al. 1998, 2004). Since this diorite yields zircon U-Pb ages of 634±2Ma (Katz et al. 1998) and 630±3Ma (Stein and Goldstein 1996), these andesite dikes must have been intruded respectively just prior to, and just after, ~632Ma (Katz et al. 2004).

The Elat Granite, which outcrops to the west and north of Elat (fig. 4), forms several undeformed plutons of red porphyritic granite consisting of very sodic plagioclase (up to 50%), microcline (15–30%), and quartz (about 25%), with small quantities of biotite and some muscovite, and apatite, zircon and iron oxides as minor accessories (Garfunkel 1980; Halpern and Tristen 1981). The texture of this calc-alkaline granite is generally equigranular, with no foliation and almost no mineral lineation. The coexistence of sodic plagioclase with non-perthitic microcline (K-feldspar) indicates sub-solvus crystallization at pressures exceeding 3–5kbar, that is, at a depth of 10–15km (Seck 1971). At such pressures crystallization of plagioclase before quartz indicates a low (few %) water content (Wyllie et al. 1976). The granite near the contacts is very contaminated. Migmatites are developed along some contacts with the schists, while contacts with the metabasites and Taba Gneiss are characterized by fracturing of the host rocks which are invaded by apophyses of granite. Feldpathization is common along the contacts. The plutons of the Elat Granite are grossly concordant with the regional structure of the enclosing rocks in spite of small scale complications of contacts. The metamorphics tend to dip away from the granite plutons, suggesting some shouldering aside of the country rocks by the granite bodies, which were thus intruded after deformation of the schists and gneisses (fig. 5). This is confirmed by Rb-Sr age determinations

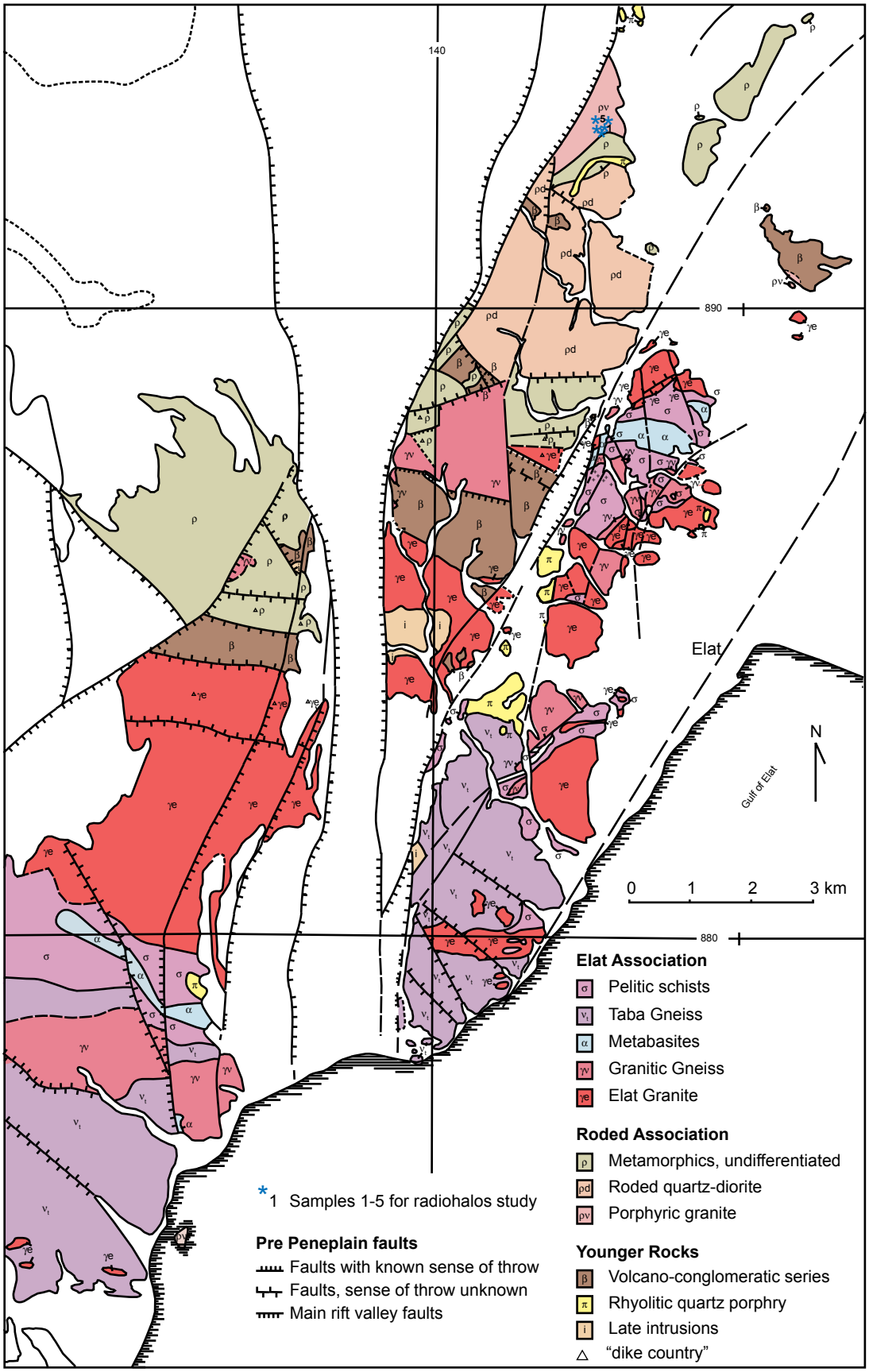

Fig. 4. The Precambrian (pre-Flood) crystalline basement (metamorphic and igneous) rocks in the Elat area of southernmost Israel (after Garfunkel 1980; Sneh et al. 1998). The locations of the samples collected from Shehoret Canyon for the radiohalos study are shown in the far north of the map area.

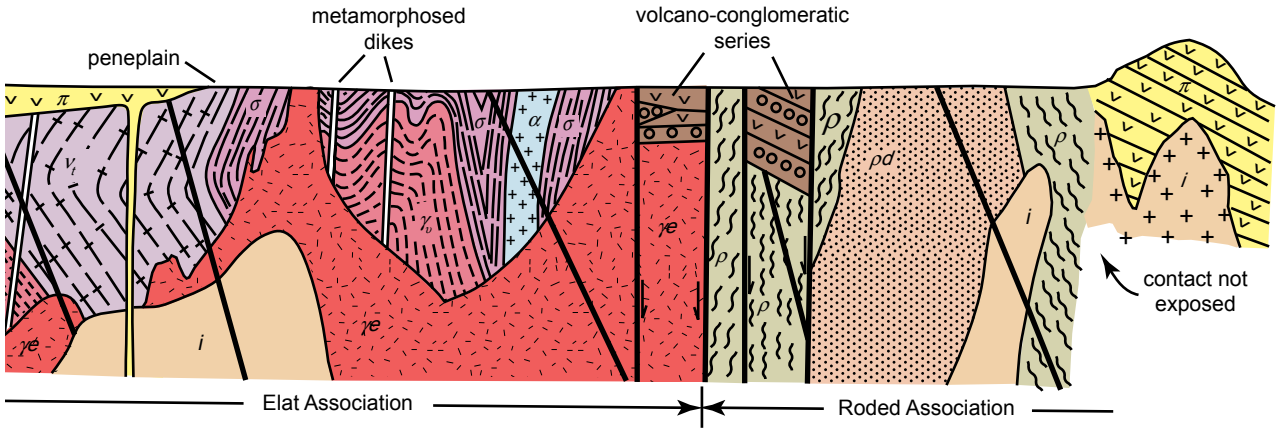

Fig. 5. A schematic geologic cross-section depicting the relationships between the various metamorphic and igneous Precambrian (pre-Flood) basement rock units in the Elat area of southernmost Israel (after Garfunkel 1980). The symbols and colors for the rock units are the same as in Fig. 4.

(Halpern and Tristen 1981). Several whole-rock analyses of the granite plotted on a 590 Ma reference isochron, while the constituent minerals yielded a mineral isochron age of 597±1 Ma. Subsequently, Stein and Goldstein (1996) obtained a Rb-Sr isochron age for the Elat Granite of 600 Ma, while Cosca, Shimron and Caby (1999) obtained an Ar-Ar plateau age of 597±1 Ma for biotite from the Elat Granite.

The Roded Association (or Terrain)

This rock suite has been relatively little studied. Garfunkel (1980) reported that there are hardly any rock types in common with the spatially adjacent Elat Association. Furthermore, the structural trend in the Roded Association rocks is close to N-S, almost perpendicular to that found in the rocks of the Elat Association. The distribution of the main Roded rock types is shown in Fig. 4 and their spatial relationships in Fig. 5. The undifferentiated metamorphics include schists, gneisses and migmatites. Table 1 lists the main Roded rock types.

The schists are variable in composition. In the north they consist essentially of plagioclase (andesine), biotite and hornblende, though some layers contain little or no biotite. In the south the schists consist of sodic plagioclase, quartz, biotite and some muscovite, while hornblende is rare or absent. Garnet is often present. Some beds contain more than 50% quartz. Secondary epidote, chlorite and sericite are widespread. The texture consists of equigranular granoblastic mosaics. The southern schists are obviously pelitic metasediments somewhat similar to those of the Elat Association and have even been designated as Elat Schist by Gutkin and Eyal (1998), whereas those in the north are quite different and may be meta-volcanics. K-Ar dating of biotite from a schist sample yielded an age of 715±9 Ma (Katz et al. 1998).

Several types of gneisses occur, mainly to the west of the schists. They generally have a quartz-dioritic or tonalitic composition, with up to 15% biotite, and frequently also some hornblende which may contain quartz inclusions. Secondary chlorite, epidote and iron oxides have developed mainly at the expense of the mafic minerals, and rarely does secondary muscovite occur. Some relatively large rectangular plagioclase crystals may be relicts of an igneous protolith. However, most plagioclase crystals are polygonal and form granoblastic mosaics, or slightly elongated aggregates. The mafic minerals often form aggregates which produce the foliation and lineation. Locally the gneisses are folded on a scale of a centimeter to several meters. In places the gneisses are banded, mainly close to the migmatite areas. Often the normal simple mineral mosaics here pass into crystals with complicated shapes and variable sizes, sutured textures very characteristic of migmatites. The gneisses were probably derived from rather homogeneous quartz-dioritic to tonalitic plutons.

The migmatites are widespread in several locations, occurring on the periphery of the Roded Quartz-Diorite pluton (fig. 4 and below). The rock consists of schist layers, often feldspathized, and quartz-plagioclase layers from 1 mm to several centimeters thick. Biotite layers are common. In one area the schist beds are often without quartz. The grain size is very variable, and sutured textures are very common. Intricate mesoscopic folding is very conspicuous. In another area this Roded Migmatite has been subdivided into two types—mildly folded migmatites and intensely folded migmatites (Gutkin and Eyal 1998). They are described as dark, banded rocks showing well-developed layers of leucosomes and melanosomes ranging in thickness from a few millimeters to tens of centimeters. The melanosomes consist of quartz (30–40%), plagioclase (20–30%) and biotite (20–40%), but in the mildly folded migmatites up to 15% garnet is present, whereas it is rare in

Table 1. Precambrian crystalline basement rock units in southern Israel.

Geographic Region	Rock Units	Constituents	Radioisotope Ages
Timna Igneous Complex	Quartz monzodiorite	Plagioclase, orthoclase, quartz and biotite, with some hornblende	599.3±2.0 Ma (zircon U-Pb)
	Alkali granite	Perthite, orthoclase, albite and quartz, with biotite	609±10 Ma (zircon U-Pb) 592±7 Ma (Rb-Sr isochron)
	Monzodiorite	Plagioclase, orthoclase, amphibole and biotite	610±8 Ma (zircon U-Pb) 592±7 Ma (Rb-Sr isochron)
	Olivine norite (gabbro)	Olivine, orthopyroxene, amphibole, biotite, magnetite and accessories	611±10 Ma (zircon U-Pb)
	Porphyritic granite	Plagioclase, orthoclase, quartz, perthite and some biotite	625±5 Ma (zircon U-Pb)
Elat Association (or Terrain)	Elat Granite	Sodic plagioclase, microline and quartz, with biotite and some muscovite	597±1 Ma (Rb-Sr mineral isochron) 600 Ma (Rb-Sr isochron) 597±1 Ma (Ar-Ar plateau age)
	Schistose dikes	Plagioclase, biotite and hornblende, with quartz minor or absent	596±2 Ma (amphibole Ar-Ar plateau age) ~632 Ma (host's zircon U-Pb)
	Shahmon Metabasites	Hornblende metagabbro to biotite hornblende metadiorite	642 Ma and 640±10 Ma (zircon U-Pb) 632 Ma (mean amphibole Ar-Ar plateau age)
	Elat Granite Gneiss	Quartz, oligoclase and alkali feldspar, with 5–15% biotite	744±5 Ma (zircon U-Pb)
	Taba Gneiss	Quartz, oligoclase and biotite, rarely with hornblende or microcline	768±9 Ma to 782±9 Ma (zircon U-Pb)
	Elat Schist	Quartz, oligoclase-andesine, biotite and some muscovite	807±35 Ma (Rb-Sr isochron) 800±13 Ma to 813±7 Ma (zircon U-Pb)
Roded Association (or Terrain)	Roded Quartz-Diorite	Oligoclase-andesine, quartz, biotite and hornblende, with minor microcline	634±2 Ma (zircon U-Pb) 617±11 Ma and 647±20 Ma (amphibole and biotite K-Ar)
	Migmatites	Melanosomes—quartz, plagioclase and biotite, sometimes with garnet or muscovite Leucosomes—quartz and plagioclase	720 Ma (zircon U-Pb)
	Amphibolites and mafic schists	Hornblende and plagioclase, with biotite and sometimes quartz	724±7 Ma (amphibole K-Ar)
	Gneisses	Plagioclase, quartz and biotite, frequently with hornblende	
	Schists	Andesine, biotite, hornblende and quartz, sometimes with garnet and muscovite	715±9 Ma (biotite K-Ar)

the intensely folded migmatites, which instead contain 10–20% muscovite. The leucosomes are predominantly quartz and plagioclase. The absence of K-feldspar from the leucosomes is inconsistent with derivation as a partial melt of the neighboring biotite-bearing rocks (Winkler 1979). Thus the migmatites were probably formed by metamorphic differentiation calculated to have occurred at approximately 600°C and 4.5 kbar, based on the analysed compositions of garnets and the muscovite-plagioclase geobarometer respectively (Gutkin and Eyal 1998). Zircon U-Pb dating of the migmatites has yielded an age of 720 Ma (Gutkin and Eyal 1998).

Regular bands of biotite-quartz-plagioclase schists, hornblende-biotite schist and amphibolites cross the gneisses or are adjacent to them (Katz et al. 1998). These have been interpreted as probably metamorphosed dikes, similar to those in the Elat

Association. In some places separate small bodies of metagabbro and amphibolite have been mapped (Gutkin and Eyal 1998). Their foliation and lineation are parallel to their walls. Furthermore, the gneisses contain a variety of irregular schist inclusions which may range from mica schists through hornblende schists to amphibolites. They are often deformed. These may be in part xenoliths or metamorphosed and dismembered minor intrusions. K-Ar dating of amphibole from an amphibolite sample yielded an age of 724±7Ma (Katz et al. 1998).

The Roded Quartz-Diorite (figs. 4 and 5, and table 1) consists of variable amounts of plagioclase (oligoclase-andesine) (50–70%), quartz (up to 20%), biotite (up to 25%), hornblende (up to 15%), and minor microcline (up to 5%). Chlorite, iron oxides, epidote, sericite and sometimes calcite replace the mafic minerals and plagioclase. The mafic minerals form aggregates, which are often elongated, while tabular plagioclase crystals sometimes tend to be oriented. These features may produce a weak foliation which trends roughly N-S. In at least one area this unit has been divided into a quartz-diorite gneiss and a quartz-diorite, even though both are homogeneous and have similar mineralogical and chemical compositions (Gutkin and Eyal 1998). Mafic stringers and elongated xenoliths, locally quite abundant, are arranged parallel to the foliation. In places there are abrupt and cross-cutting contacts between varieties of quartz-diorite. The xenoliths are medium- to fine-grained igneous or foliated rocks, all having a mela-quartz-dioritic to mela-dioritic composition. As already described above, migmatites occur along much of the borders of the Roded Quartz-Diorite pluton (fig. 4). They contain tongues, often discordant, of a somewhat foliated rock similar to the quartz-diorite, only richer in mafic minerals. The eastern border of the pluton is grossly parallel to the structural grain of the adjacent metamorphics, but to the north and south the transition is along strike, though contacts are largely masked by faults. This quartz-diorite body is interpreted as having been formed by anatexis, and did not move far from its place of origin (Garfunkel 1980). The mosaics of polygonal quartz and untwinned plagioclase crystals and poikilitic hornblende crystals in the quartz-diorite that resemble those found in the gneisses, and the stringers of mafic minerals and the xenoliths, are probably relicts of the source rocks. The heterogeneity of the pluton suggests incomplete mixing and production of many batches of partial melt. It is also possible that a portion of the melt moved still further upwards in the crust at that time, so the present rock is a residue left behind. The bordering migmatites, though most probably formed by metamorphic differentiation, must be genetically linked to the pluton because of their spatial relationship. The foliation of the quartz-diorite probably formed by flow during emplacement. Zircon U-Pb dating of the quartz-diorite has yielded a crystallization age of 634±2Ma, while K-Ar dating of amphiboles and biotites from the same rock gave ages of 617±11Ma and 647±20Ma respectively (Katz et al. 1998). Thus the intrusion of this quartz-diorite is regarded as occurring at around 632Ma (Katz et al. 2004).

Schistose dikes, which were originally andesite (Cohen et al. 2000, Katz et al. 2004), also cut across the Roded Quartz-Diorite and are discordant to the metamorphic structure of the country rocks. Other such dikes which are concordant with the metamorphic structure do not intrude the quartz-diorite (Katz et al. 2004). Thus, due to the dating of the quartz-diorite (Katz et al. 1998; Stein and Goldstein 1996) these dikes must have been intruded just prior to, and just after, ~632 Ma (Katz et al. 2004).

A porphyritic granite (or granite porphyry) occurs in the northern part of the Roded terrain (fig. 4). This rock has many features resembling the quartz-diorite, being heterogeneous, and rich in xenoliths and in bands of mafic minerals. However, this porphyritic granite contains abundant microcline (K-feldspar) as phenocrysts, often perthitic, enclosing plagioclase, quartz and mica crystals, and it is also common in the matrix. The latter resembles the matrix of the quartz-diorite, but is richer in quartz and microcline, has a lower color index, and no hornblende. Myrmekite and replacement of plagioclase by K-feldspar are common. Migmatites are also developed along the border of this granite and contain K-feldspar in the leucosome, in contrast to the neighboring migmatites developed on the northern periphery of the quartz- diorite.

Small irregular stocks, dikes or veins of leuco-granites intrude all of already-described rock units, with sharp contacts. The compositions of these leuco-granites are quite variable, and are characterized by a low color index and a high content of K-feldspar (25–50%). The plagioclase is albite-oligoclase. The leuco-granites and the enclosing rocks are crossed by numerous fractures with displacements of less than a meter and by cataclastite bands.

The Roded Quartz-Diorite and porphyritic granite plutons, which are heterogenous, charged with inclusions, somewhat foliated and associated with migmatites, resemble deep-seated plutons, whereas the Elat Granite plutons are of the high-level type (Buddington 1959; Hutchinson 1970). This suggests that the Roded Association (or terrain) was formed deeper in the crust, which is consistent with geothermometry studies based on analysed mineral chemistries in the schists, gneisses and amphibolites (Katz et al. 1998). The

peak metamorphic pressure-temperature conditions were inferred to have been about 650°C and less than 5 kbar, probably attained by 725 Ma. Both the Elat and Roded suites of rocks though appear to record an overall similar history. In both terrains metamorphosed dikes probably distinguish an older metamorphic complex, including metasediments and completely reconstituted intrusions, from young unmetamorphosed intrusions.

Timna Igneous Complex

The most northerly outcrops of the Precambrian crystalline basement rocks are in the Timna area north of Elat (fig. 2). The intrusive rocks of the Timna Igneous Complex consists of five major plutonic and various hypabyssal lithologies (fig. 6 and table 1) (Beyth 1987; Beyth et al. 1994a; Shpitzer, Beyth, and Matthews 1991). The plutonic variants include:

1. Cumulates of olivine norite (gabbro), with up to 40% olivine, 7% orthopyroxene, 15% amphibole, 14% plagioclase, 10% biotite, 8% magnetite (and sulfides), and 6% accessories (apatite and zircon). Minor pyroxene hornblende peridotite accompanies the olivine norite.
2. Amphibole diorite, monzodiorite and monzonite, collectively mapped as monzodiorite (fig. 6), with 32–38% plagioclase, 5–35% orthoclase, 11–35% amphibole, 5–19% biotite, 4–5% magnetite (and sulfides), and 1–3% accessories.
3. Quartz monzodiorite, with 40% plagioclase, 23% orthoclase, 15% quartz, 3% hornblende, 11% biotite, 5% magnetite (and sulfides), and 3% accessories.
4. Porphyritic granite, with 44% plagioclase, 25% orthoclase, 23% quartz, 3% perthite, 3% biotite, and 2% accessories.
5. Alkali granite (pink), accompanied by alkali syenite, with 24–57% perthite, 23% orthoclase, 11–25% albite, 22–24% quartz, 3–4% biotite, 1–3% magnetite (and sulfides), and 1-2% accessories.

The hypabyssal rocks include dikes of rhyolite, andesite (potassic trachyandesites and shoshonites) (Beyth and Peltz 1992), and diabase (dolerite), as well as composite andesite-rhyolite dikes (fig. 6).

The Timna Igneous Complex is exposed over an area of about 20 km^2 around Mt. Timna (fig. 6). The alkali granite (and syenite) make up the majority of these exposures, occupying the topographically elevated parts. The lower elevations surrounding the alkali granite are built of olivine norite blocks, typically 30×30 meters, which are most probably xenoliths,

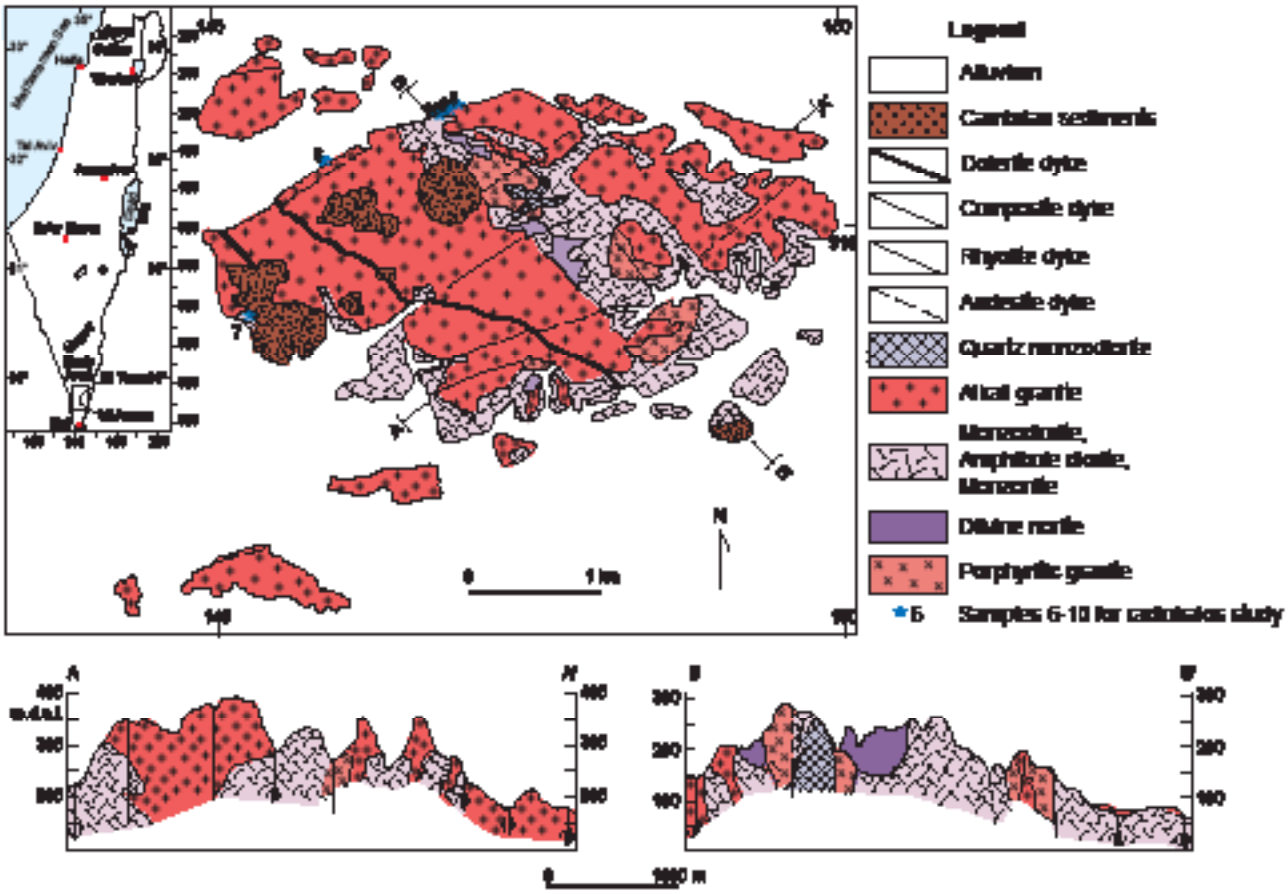

Fig. 6. Location and general geologic maps of, with two geologic cross-sections through, the Timna Igneous Complex in the Mt. Timna area of southernmost Israel (after Beyth et al. 1994a). The locations of the samples collected for the radiohalos study are shown.

engulfed by monzodiorite with diffuse contacts. The monzodiorites are very heterogeneous and appear to be differentiated from olivine norite to amphibole monzonite (Shpitzer, Beyth, and Matthews 1991). These are associated with small alkali granite stocks, while the massive part of the alkali granite and syenite overlie the monzodiorite. All these rocks are intruded into the porphyritic granite (fig. 6), which occurs as blocks of varying sizes. The youngest plutonic rock is the quartz monzodiorite which contains numerous xenoliths of all the previously mentioned (earlier) rock types. The dikes intrude this plutonic complex in three distinctive generations (Beyth et al. 1994a). The oldest one is in a N-S direction, the intermediate and dominant one is in an ENE direction, and the youngest in a NW direction (fig. 6).

Zircon U-Pb dating determinations confirm the sequence in which the intrusions were emplaced (table 1) as gleaned from the field evidence outlined above. The porphyritic granite yielded an age of 625±5Ma, and is thus clearly the oldest unit exposed at Timna (Beyth et al. 1994a). Similar ages were obtained for the olivine norite (611±10Ma), monzodiorite (610±8Ma), and the alkali granite (609±10Ma), consistent with the interpretation that these are comagmatic (Beyth et al. 1994a). The quartz monzodiorite, the youngest plutonic intrusive based on the field evidence, yielded a zircon U-Pb age of 599.3±2.0Ma, averaged from 14 grains (Beyth and Reischmann 1996). Rb-Sr data for samples of the 610Ma olivine norite, monzodiorite and alkali granite yield an apparent isochron age of 581Ma with a high MSWD of 8.5 (Beyth et al. 1994a), which is very similar to the 592±7Ma Rb-Sr isochron age obtained by Halpern and Tristan (1981) for Timna granitic rocks.

Based on whole-rock major, trace and rare earth element, and isotopic, geochemical analyses, Beyth et al. (1994a) concluded that the 625Ma porphyritic granite is a typical calc-alkaline I-type subsolvus granite with volcanic arc or collisional affinities, which was probably generated by anatexis of slightly older crust. After an apparent transitional period from such an orogenic collisional tectonic regime, a crustal extensional tectonic regime was initiated, in which a mantle-derived monzodiorite, or sanukitoid (Stern, Hansen, and Shirey 1989), magma intruded the porphyritic granite at 610Ma, forming a stratified magmatic cell. Olivine norite formed as cumulates at the bottom of the cell and were later brought up as xenoliths by late monzodioritic injections into this cell. The alkali granite formed by fractionation from this mantle-derived, LILE-enriched sanukitoid magma.

This interpretation that the olivine norite, monzodiorite and alkali granite are comagmatic is based on their field relationships and on several other lines of evidence (Beyth et al. 1994a ; Shpitzer, Beyth, and Matthews 1991). First, these are the same 610Ma age, within the analytical uncertainty. Second, their Nd and Pb isotopic compositions are consistent with the interpretation of consanguinity. Lastly, their ancillary chemical data support this interpretation. These include similar K/Rb in both the monzodiorite and alkali granite, both of which are distinct from the older porphyritic granite. Furthermore, incompatible element abundances such as Nb, Ta, Th, and Yb are inversely correlated as indices of fractionation. Thus it was concluded that the alkali granite was fractionated from the monzodiorite magma, either as a consequence of crystal fractionation or liquid immiscibility. Additionally, geothermobarometric studies using mineral chemistries indicate temperatures in the range 500–600°C and pressures less than 5kbar for all these rock types (Shpitzer et al. 1991).

The quartz monzodiorite, which is the youngest plutonic rock in the complex, suggests that this monzodioritic intrusion event ended with the intrusion of the rhyolite, andesite and rhyolite/andesite (composite) dikes (Beyth et al. 1994a). These younger hypabyssal intrusions have chemical compositions that plot with the monzodiorite and alkali granite respectively, so it is inferred that the fractionation relationship between the alkali granite and the monzodiorite was repeated on a small scale between the magmas responsible for the rhyolite and andesite dikes, and is especially well expressed in the composite ones. These dikes, which were probably feeder dikes for volcanic rocks that were later eroded, have been dated in the nearby Sinai area as 590Ma (Stern and Manton 1987).

The major diabase (dolerite) dike intruded the alkali granite, which at the time had previously been fractured and intruded by rhyolite, andesite and andesite-rhyolite composite dikes (fig. 6), so it is the youngest igneous event in the Timna complex (Beyth and Heimann 1999). This has been confirmed by whole-rock K-Ar and Ar-Ar determinations. The mean K-Ar age obtained, based on two samples, was 546.3±10.1Ma (Beyth and Heimann 1999). The total Ar-Ar age of one sample was 527.2Ma, whereas its Ar-Ar plateau age was 531.7±4.6Ma. Based on the argument that the plateau age is the best estimate of a sample's age, it was concluded that this diabase dike was intruded at 531.7±4.6Ma (532Ma). Geochemically similar diabase dikes are also found at Mt. Amram, where alkali granite, monzonite and quartz monzonite are also exposed 13km south of Mt. Timna (Beyth et al. 1994b; Kessel, Stein, and Navon 1998), elsewhere in the Sinai (Friz-Topfer 1991) and in nearby Jordan (Jarrar, Wachendorf, and Saffarini 1992). The dikes in Jordan, though, yielded a K-Ar age of 545±13Ma, similar to the K-Ar age of 546.3±10.1Ma obtained for

the Timna diabase dike. Nevertheless, the ages for these dikes are close to 542 Ma, the defined date of the Cambrian/Precambrian boundary (Gradstein, Ogg, and Smith 2004), although Jarrar, Wachendorf, and Zachmann (1993) compiled an age of 530±10 Ma for the Cambrian/Precambrian peneplain boundary in this Sinai-Jordan region. That the diabase dike at Timna was intruded before this peneplanation occurred is confirmed by the lack of any contact metamorphism in the overlying lower Cambrian sandstone of the Amudei Shelomo Formation (Beyth and Heimann 1999).

All the intrusive rocks of the Timna Igneous Complex have subsequently been subtly altered. A chemical remnant magnetic direction similar to the sub-recent field (Miocene to present) was identified in the olivine norite, monzodiorite, quartz monzodiorite and dikes of various compositions (Marco et al. 1993). The magnetic mineral assemblage of magnetite and Ti-magnetite in these rocks was thus found to have been altered by oxidation and hydration to secondary hematite and goethite. Subsequent investigations (Beyth et al. 1997; Matthews et al. 1999) showed that these alteration processes had also resulted in significant modification of both the mineralogy and the oxygen and hydrogen isotope compositions of these Precambrian igneous rocks, consistent with hydrothermal alteration under warm conditions (<200°C) at low to medium water/rock ratios, followed by weathering or supergene alteration by local meteoric waters. This hydrothermal activity occurred before uplift and erosion exposed these basement rocks during the early stages of tectonic activity along the Dead Sea rift in the middle Miocene, presumably at the very end of the Flood event. The most likely fluid source would have been the basinal brines in the overlying Flood-deposited sedimentary rocks, the movement of which into the Precambrian basement rocks below was triggered by onset of the Dead Sea rifting. This also resulted in uplift, so the retreating Flood waters would then have eroded away some of these sedimentary rocks, exposing the Precambrian igneous rocks to weathering to produce the present outcrops.

General latest Precambrian igneous activity

Within the Elat and Roded terrains are found isolated remnants of latest Precambrian igneous activity that likely coincides with the progressive emplacement of the Timna Igneous Complex, especially the hypabyssal dikes. Kessel, Stein and Navon (1998) delineated three distinct swarms of dikes that cut across both the Elat massif (which includes both the Elat and Roded terrains) and the Amram massif (which is situated between the Elat massif and the Timna Igneous Complex to the north). The oldest dike suite consists of andesitic to rhyolitic dikes that strike N-S and geochemically are calc-alkaline. The second group strikes NE-SW and contains tholeiitic basaltic to rhyolitic dikes that cross-cut the older calc-alkaline dikes. Both these suites of dikes are commonly 0.5–5.0 m wide, and have not been dated. However, dikes of similar chemistry and stratigraphic emplacement from nearby massifs show a range of ages between 600 and 540 Ma (Beyth et al. 1994a ; Bielski 1982), the calc-alkaline dikes likely corresponding to the last phase of the emplacement of the Elat Granite. Finally, the youngest group of dikes, not represented in the Elat massif, consists of two NW-SE striking alkali basaltic dikes approximately 60 m wide in the Amram massif. These diabase (dolerite) dikes are similar in orientation, appearance and chemical composition to the diabase (dolerite) dike in the Timna massif which also cuts across dikes of two older swarms similar to the calc-alkaline and tholeiitic dikes in the Elat and Amram massifs (Beyth et al. 1994a, b). Beyth and Heimann (1999) concluded that Timna diabase dike was intruded at 532 Ma.

Gutkin and Eyal (1998) also recognized the same older two suites of dikes in the Mt. Shelomo area, 5 km northwest of Elat, as described by Kessel et al. (1998). The first (oldest) group forms a swarm of hundreds of dikes, a few meters thick, which in many cases cross one another, but are usually only tens of meters long. These dikes similarly range from andesite or andesitic basalt to dacitic and rhyolite-dacitic. The second (younger) swarm cross-cuts all the metamorphic and plutonic country rocks as well as the earlier dikes, and consists of a few large rhyolitic dikes, one of which is 10–30 m thick and more than 3 km long.

Garfunkel (1980) noted a volcanic neck in the southern part of the Ramat Yotam area about 2 km west of Elat, containing tuffs and surrounded by a hydrothermally-altered breccia of Taba Gneiss. Subsequently, Eyal and Peltz (1994) mapped the structure of what they recognized as a deeply eroded ash-flow caldera, now called the Ramat Yotam Caldera. Although faulted after eruption, when restored to its original position this elliptically-shaped caldera would have had a diameter of about 2×3 km. Composed mainly of silicic ignimbrites, the thickness of the exposed composite section is about 250 m.

These silicic ignimbrites of the Ramat Yotam Caldera are the southernmost representatives of the silicic Elat volcanic field (Eyal and Peltz 1994), remnants of which are exposed further north in the Shehoret Canyon area and at Mt. Amram, as well as to the northwest at Mt. Neshef. These outliers of the Elat volcanic field cover some 13 km^2. Garfunkel (1980) claimed that the Ramat Yotam Caldera could have been the source of these dacitic or rhyodacitic

ignimbrites found further north, so Bielski (1982) dated many of these tuffs and obtained a whole-rock Rb-Sr isochron age of 548±4 Ma. Segev (1987) though regrouped these and other similar volcanic rocks according to their individual sites and recalculated their Rb-Sr isochron ages, obtaining ages of 529±12 Ma (Mt. Neshef), 548±4 Ma (Shelomo area), and 532±7 Ma (for Mt. Neshef and three other nearby sites in northeastern Sinai and southwestern Jordan combined). Clearly, given the spatial and temporal proximity of these explosively-erupted silicic volcanic rocks to the Precambrian-Cambrian boundary and therefore the beginning of the Flood event (see below), and the unreliability of the radioisotope dating methods (Snelling 2000; Vardiman, Snelling, and Chaffin 2005), it is quite likely that the explosive eruption of these rhyolitic volcanics and ignimbrites, and the intrusion of the associated dikes, were related to the initiating stage of the "breaking up" of the "fountains of the great deep."

The Arabian-Nubian Shield

These Precambrian basement granites and metamorphics in southern Israel (and in neighboring Jordan) are recognized as the northernmost exposed extent of the Arabian-Nubian Shield. This Precambrian shield area outcrops along the coastlines of the Gulf of Elat (or Aqaba) and across into the Sinai Peninsula (Kröner, Eyal, and Eyal 1990), and extends along either side of the Red Sea. On the African coastline is the Nubian Shield of Egypt and Sudan that also extends through Eritrea into northern Ethiopia, while along the opposite Red Sea coastline is the Arabian Shield of Saudi Arabia that extends into Yemen (Be'eri-Shlevin et al. 2009; Stacey and Hedge 1984; Sultan et al. 1990). That these two shield areas were once joined together as the Arabian-Nubian Shield has been established by reconstructing the pre Red Sea opening configuration, the two areas matching along the Red Sea rift line.

The geochronologic and isotopic evidence available confirms that the Arabian-Nubian Shield was originally part of the Precambrian supercontinent Rodinia. The oldest rock so far established is a granodiorite in Saudi Arabia that has yielded a Paleoproterozoic zircon U-Pb concordia age of 1,628±200 Ma (Stacey and Hedge 1984), which was concluded to probably be its emplacement age. Furthermore, the Pb isotopes show that these 1,630 Ma crustal rocks could have inherited material from an older, probably Archean, source at the time of their formation. This is consistent with contemporaneous addition of mantle material that considerably modified the Rb-Sr and Sm-Nd systems so that they now yield similar, or only slightly older, 1,600–1,800 Ma apparent ages.

In the northernmost Arabian-Nubian Shield in the Sinai Peninsula, detritral zircons within a schist, coupled with whole-rock Nd isotopic analyses, have provided evidence of pre-Neoproterozoic crust (Be'eri-Shlevin et al. 2009). The detrital zircon age population was bimodal, with concordia ages in the 1,000–1,100 Ma range. The whole-rock Nd isotopic value was significantly lower than for juvenile Neoproterozoic rocks in the region, which was interpreted as implying that 1 Ga age crust was incorporated into the northernmost Arabian-Nubian Shield. The $\delta^{18}O$ (zircon) values were also consistent with supracrustal recycling being involved in the formation of this 1,000–1,100 Ma crust.

The Arabian-Nubian Shield, consisting of a diverse variety of metamorphosed sedimentary and volcanic rocks intruded by granitic and other plutonic rocks, thus has an apparent long history somewhat similar to the Precambrian crystalline basement rocks exposed in the inner gorges of the Grand Canyon in northern Arizona (Beus and Morales 2003). Within the biblical framework of earth history the Creation Week was a period of just six literal days in which God's sequential creative activities produced virtually instantaneously and therefore catastrophically a fully-functioning earth with an apparent history if viewed only in terms of human experience today (Snelling 2009). Of greatest relevance geologically was God's creative work on Days One and Three, when He initially created and formed the earth, likely with an initial crust divided from the mantle and core, and then subsequently further formed and structured the crust to produce the dry land, likely as a supercontinent, perhaps that identified as Rodinia by the conventional geologic community. The Arabian-Nubian Shield would have been a part of the pre-Flood supercontinent, thus designating these Precambrian crystalline basement rocks exposed in southern Israel as likely Creation Week rocks, similar to their equivalents in the Grand Canyon (Austin 1994).

If some credence is given to the radioisotope age determinations of these Precambrian metamorphic and granitic rocks of the Elat area in southern Israel (fig. 4 and table 1) as already detailed, then, due to the systematic pattern of radioisotope ages that would result from an episode of accelerated nuclear decay during the Creation Week (Snelling 2005b; Vardiman, Snelling, and Chaffin 2005), there are significant differences between these rocks and their equivalents in the Grand Canyon. There is no doubt that they form the crystalline basement foundations to the stratigraphic succession of sedimentary rock units in Israel (fig. 3). However, they yield radioisotope ages of 800-813 Ma for the Elat Schist to 600–625 Ma for the Elat Granite and Timna Igneous Complex, placing them according to Snelling (2009) in the pre-Flood era between

Creation Week and the Flood, at the time when the Neoproterozoic Chuar Group sediments were being deposited in the Grand Canyon area (Austin 1994). In the Grand Canyon the basement metamorphic and granitic rocks yield Paleoproterozoic radioisotope ages of 1.73–1.75 Ga (metamorphics) and 1.84 Ga and 1.66–1.74 Ga (granites) (Beus and Morales 2003), placing them in the early part of the Creation Week (Austin 1994; Snelling 2009), and are overlain by the Mesoproterozoic Unkar Group sediments and lavas that were likely mid-late Creation Week rocks. Thus if these metamorphic and granitic rocks in southern Israel are to be placed in the biblical framework of earth history based only on their radioisotope ages, then they would have to represent metamorphism and magmatism that occurred during the pre-Flood era, while people and animals were living elsewhere on the supercontinental land surface. This seems unlikely, so clearly using relative radioisotope ages is not always a reliable indicator of where rock units should be placed in the biblical framework of earth history, as mixing and inheritance are still processes that can perturb the radioisotope systems (Snelling 2000, 2005b). Indeed, crustal recycling of radioisotopes and mixing of mantle components in the Arabian-Nubian Shield is well documented (Be'eri-Shlevin et al. 2009; Kröner, Eyal, and Eyal 1990; Stacey and Hedge 1984; Sultan et al. 1990), as already indicated above.

Radiohalos

It hardly seems necessary to defend the catastrophic formation of these metamorphic and granitic rocks in southern Israel if they were formed by God's creative processes during the Creation Week as God assembled the dry land of the pre-Flood supercontinent. However, it can be demonstrated that both regional metamorphism and granite magmatism are catastrophic processes (Snelling 1994, 2007, 2009). One important indicator that imposes severely short time constraints on these processes is the formation within these rocks of polonium radiohalos (Snelling 2005a, 2007, 2008b, c; Snelling and Armitage 2003; Snelling and Gates 2009). So it is to be expected that polonium radiohalos would be present in these Precambrian granitic rocks in southern Israel.

The Roded Porphyritic Granite and the Timna Igneous Complex's monzodiorite and alkali granite were sampled (five samples from each area) (see figs. 4 and 6). Outcrops sampled in the Shehoret Canyon and Timna areas respectively are shown in Fig. 7. The samples were processed and biotite flakes mounted for microscope examination to count their contained radiohalos according to the method outlined by Snelling and Armitage (2003). Fig. 8 provides photo-micrographs of the different sampled rock units showing their mineralogy and textures, while Fig. 9 shows some of the radiohalos found in the biotites of these samples. All five samples of the Roded Porphyritic Granite contained ^{210}Po radiohalos, while three samples each contained a ^{238}U radiohalo, with an abundance range of 0.06–0.76 radiohalos per slide in the separated and

Fig. 7 (p. 181). Outcrops sampled for the radiohalos study (locations shown in Figs. 4 and 6). (a) General view of Shehoret Canyon, looking "upstream." (b) Sample IGR-1 collection site from the Roded Porphyritic Granite exposed in Shehoret Canyon. (c) Sample IGR-3 collection site from the Roded Porphyritic Granite in Shehoret Canyon. (d) The Roded Porphyritic Granite at the sample IGR-5 collection site showing the dark enclaves of mafic minerals. (e) General view of the alkali granite of the Timna Igneous Complex, in the Timna mountains, opposite and above the sample IGR-10 collection site. (f) The alkali granite of the Timna Igneous Complex at the sample IGR-6 collection site. (g) The monzodiorite of the Timna Igneous Complex at the sample IGR-7 collection site. (h) the monzodiorite of the Timna Igneous Complex at the sample IGR-10 collection site.

Fig. 8 (p. 182). Photo-micrographs of some of the samples examined in the radiohalos study. All are at the same scale (20× or 1 mm = 40 μm) and as viewed under crossed polars, (a) Roded Porphyritic Granite, sample IGR-1: plagioclase (with multiple twinning), microcline, and biotite (colored flakes showing alteration). (b) Roded Porphyritic Granite, sample IGR-4; plagioclase (partly extinguished), microcline, biotite (altered), and quartz (small grains). (c) Roded Porphyritic Granite, sample IGR-5: plagioclase, microcline, and biotite. (d) Timna alkali granite, sample IGR-6: perthite (intergrown plagioclase and orthoclase), biotite (altered), and orthoclase. (e) (f) Timna monzodiorite, sample IGR-7: plagioclase, orthoclase, perthite, biotite, and magnetite (black). (g) (h) Timna monzodiorite, sample IGR-10: plagioclase, orthoclase, biotite, amphibole (altered) and magnetite.

Fig. 9 (p. 183). Photo-micrographs of some of the radiohalos identified and counted in the radiohalos study (see table 2). All are at the same scale (40× or 1 mm=20μm) and as viewed in plane polarized light. (a) Roded Porphyritic Granite, sample IGR-1, slide 32, three ^{210}Po radiohalos and one ^{238}U radiohalo (top). (b) Roded Porphyritic Granite, sample IGR-1, slide 32, three ^{210}Po radiohalos. (c) Roded Porphyritic Granite, sample IGR-2, slide 15, three ^{210}Po radiohalos and one partial ^{238}U radiohalo (to the left on the edge of the grain). (d) Timna Monzodiorite, sample IGR-7, slide 7, one ^{210}Po radiohalo (upper left), three ^{238}U radiohalos (bottom center and right), and several elongated fluid inclusions. (e) Timna Monzodiorite, sample IGR-7, slide 13, four ^{210}Po radiohalos plus fluid inclusions. (f) Timna Monzodiorite, sample IGR-7, slide 13, one ^{210}Po radiohalo (lower left), one ^{238}U radiohalo (upper right) and fluid inclusions. (g) Timna Monzodiorite, sample IGR-10, slide 30, three ^{210}Po radiohalos, with one of them around a fluid inclusion. (h) Timna Monzodiorite, sample IGR-10, slide 24, two ^{210}Po radiohalos, with one around a fluid inclusion.


(a)


(b)


(c)


(d)


(e)


(f)


(g)


(h)

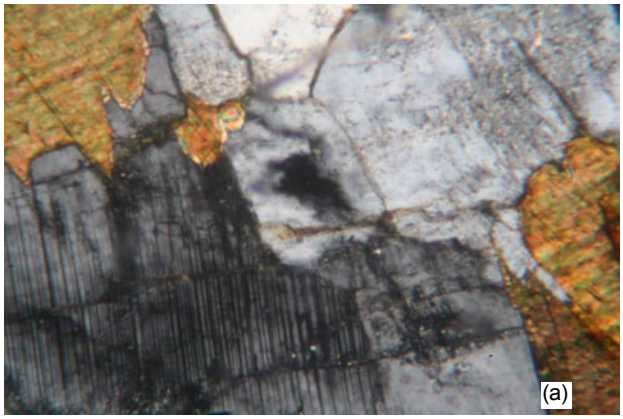
(a)

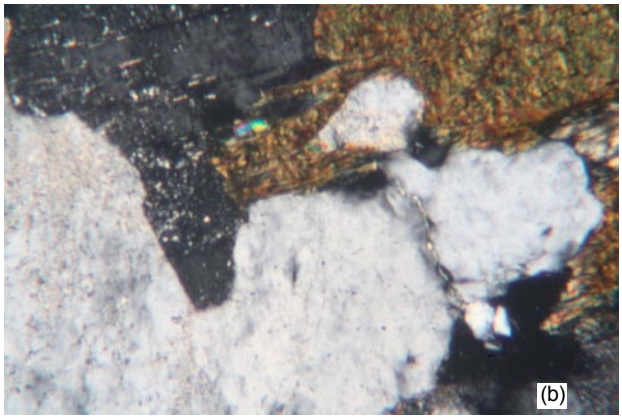
(b)

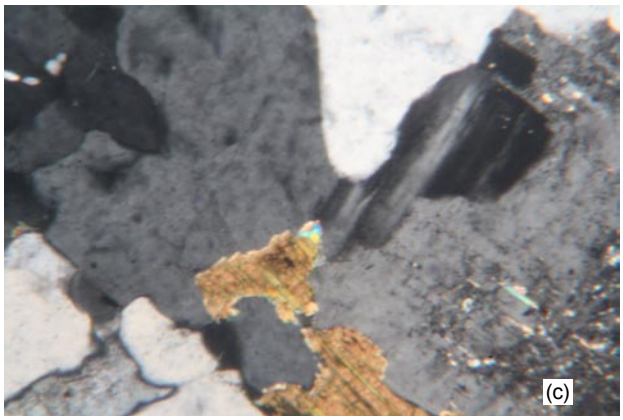
(c)

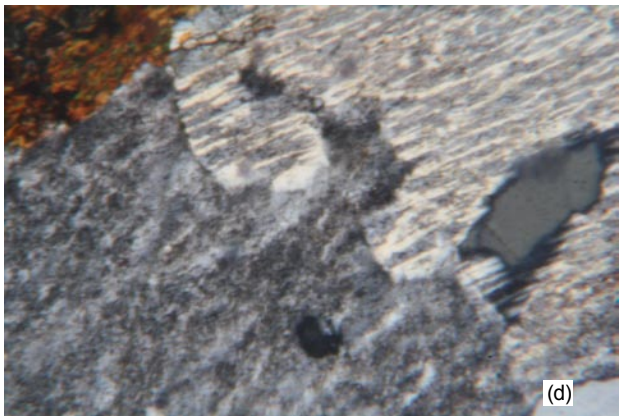
(d)

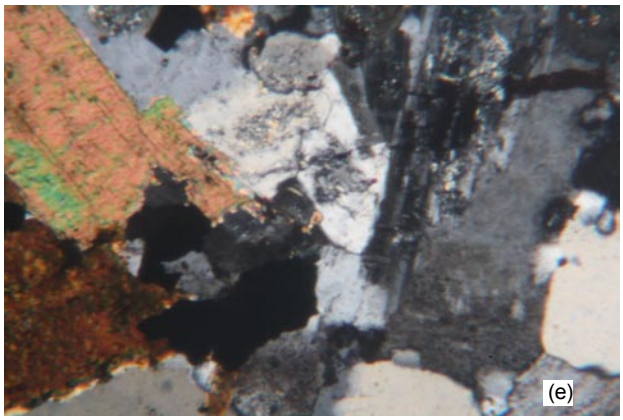
(e)

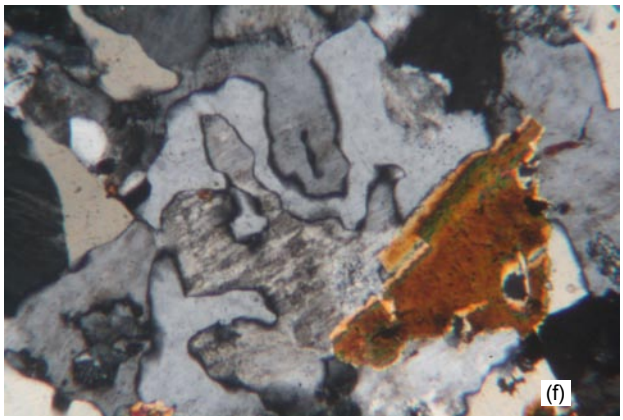
(f)

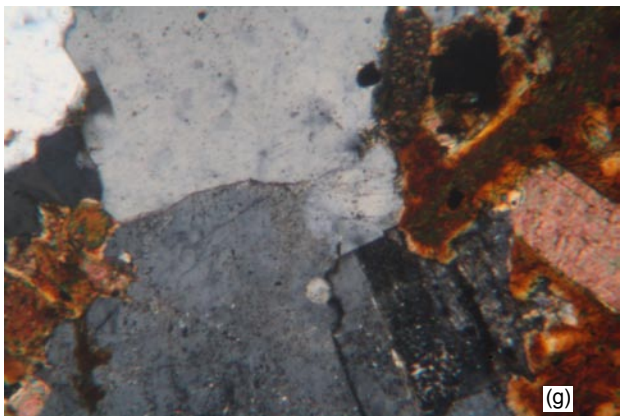
(g)

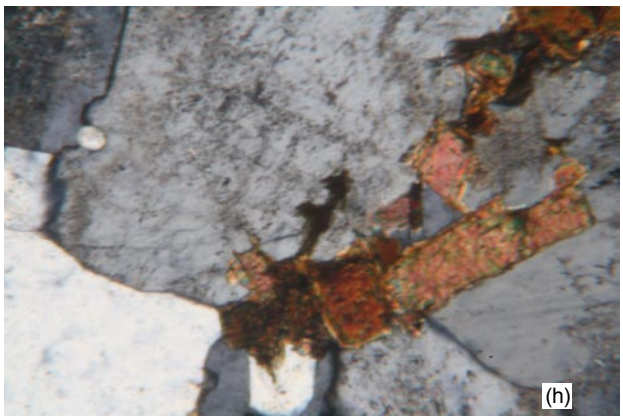
(h)

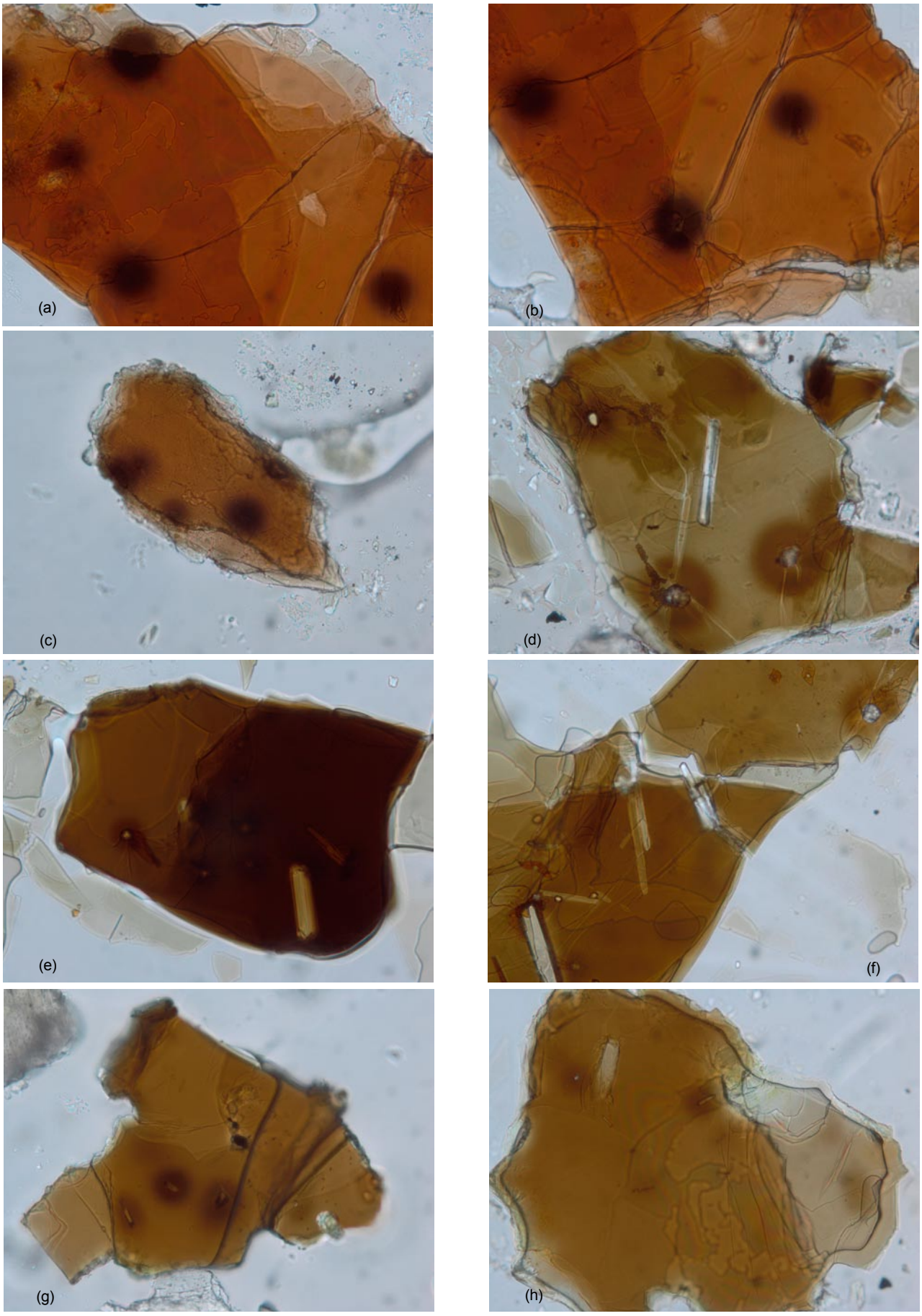
(a)
(b)
(c)
(d)
(e)
(f)
(g)
(h)

Table 2. Radiohalos in the Precambrian Roded Porphyritic Granite, and alkali granite and monzodiorite from the Timna Igneous Complex.

Location	Rock Unit	Sample Number	Number of Slides	Radiohalos					Number of Radiohalos per Slide	Number of Po Radiohalos per Slide	Ratio ^{210}Po:^{238}U
				^{210}Po	^{214}Po	^{218}Po	^{238}U	^{232}Th			
Shehoret Canyon	Roded Porphyritic Granite	IGR-1	50	37	—	—	1	—	0.76	0.74	37:1
		IGR-2	50	4	—	—	1	—	0.10	0.08	4:1
		IGR-3	50	3	—	—	—	—	0.06	0.06	—
		IGR-4	50	11	—	—	—	—	0.22	0.22	—
		IGR-5	50	8	—	—	1	—	0.18	0.16	8:1
Timna Park, and Timna Mountains	Timna alkali granite	IGR-6	50	—	—	—	—	—	—	—	—
		IGR-8	50	—	—	—	—	—	—	—	—
	Timna monzodiorite	IGR-7	50	62	—	—	3	—	1.30	1.24	21:1
		IGR-9	50	—	—	—	—	—	—	—	—
		IGR-10	50	72	—	—	3	—	1.50	1.44	24:1

mounted biotite flakes (table 2). In contrast, only two samples from the Timna Igneous Complex, both monzodiorite, contained radiohalos, but both ^{210}Po and ^{238}U radiohalos, with a higher abundance range of 1.30–1.50 radiohalos per slide (table 2).

The ratios of ^{210}Po:^{238}U radiohalos are high and typical of Precambrian (pre-Flood) granitic rocks, as are the low radiohalos abundances (Snelling 2005a). This is because these granitic rocks have likely had all the radiohalos that formed in them initially, when the original magmas crystallized and cooled, subsequently annealed by temperatures of 150°C and above generated by their burial below the thick overlying sedimentary rock sequence deposited during the Flood (Snelling 2005a). Thus the radiohalos now observed in these granitic rocks were likely formed by the passage of further hydrothermal fluids through them during the Flood, for which there is abundant evidence in them, namely, the chloritization of biotites and sericitization of feldspars, as observed in the thin sections (fig. 8).

Even though all the rock units sampled (table 2) show the effects of alteration subsequent to their original crystallization, there are obvious differences in their radiohalo abundances. The Timna alkali granite contains no radiohalos, the Roded Porphyritic Granite a few radiohalos, and the Timna monzodiorite many more radiohalos. Assuming that all these granitic rock units after crystallization were subject to temperatures above 150°C, due to subsequent deeper burial by thick overlying Flood-deposited sedimentary sequences, so that all the radiohalos produced in them when they originally crystallized were annealed, then these relative differences in radiohalo abundances in these rock units could be due to them subsequently experiencing different quantities of hydrothermal fluids during the Flood event. That greater abundances of radiohalos are produced by greater quantities of hydrothermal fluids has been well established and verified, both in granitic rocks (Snelling 2005a, 2008c; Snelling and Gates 2009) and in metamorphic rocks (Snelling 2008a, b).

It can easily be demonstrated that these granitic rock units in southern Israel were buried under thick sedimentary sequences during the Flood. In the areas where these samples were obtained, the unconformity between these granitic rock units and the overlying Flood-deposited sedimentary sequence is exposed (fig. 10). Thus at some stage during the Flood, as or after the overlying sedimentary sequence was deposited, the basinal brines in these deeply buried basal (Cambrian) sediments just above the unconformity would likely have been heated sufficiently to become hydrothermal fluids. This has been confirmed by evidence that temperatures in the overlying Cambrian sandstone reached as high as 200°C (Vermeesch, Avigad, and McWilliams 2009). These hydrothermal fluids would then have circulated down into the underlying Precambrian crystalline basement rocks. That this has certainly occurred in the Timna Igneous Complex rocks has been confirmed by paleomagnetic and isotopic evidence (Beyth et al. 1997; Marco et al. 1993; Matthews et al. 1999). And since it occurred at the end of the Flood during the early triggering stages of tectonic activity along the Dead Sea rift, which is adjacent to both sampled areas, then most of the Precambrian granitic and metamorphic rocks would have been affected similarly. However, Beyth et al. (1997) showed that the monzodiorite was more altered than the alkali granite by these circulating hydrothermal fluids. Thus it seems reasonable to conclude that the degree of alteration corresponds to the volume of hydrothermal fluids which circulated through these rocks. This in turn would be consistent with the earlier proposal that the greatest abundance of radiohalos in the monzodiorite is due to a greater volume of hydrothermal fluids circulating through it

Fig. 10. The unconformity between the Precambrian (pre-Flood) crystalline basement rocks and the overlying Cambrian sandstone at the base of the Flood sediment sequence. (a) (b) Above Shehoret Canyon (c) (d) Below Solomon's Pillars in the Timna area, close by the sample IGR-7 collection site (see fig. 6 for location).

during the Flood. If this conclusion is correct, then it would imply that the Roded Porphyritic Granite in the Shehoret Canyon area, with its consistent low radiohalos abundance, had slightly more hydrothermal fluid-flow through it than the Timna alkali granite with its complete lack of radiohalos.

Biotite, which hosts the radiohalos in the Roded Porphyritic Granite and the Timna monzodiorite and alkali granite, is also present to abundant in the Elat Schist, the Taba Gneiss, the Elat Granite, and the Elat Granite Gneiss, as well as the metadiorites of the Shahmon Metabasites, of the Elat Association, in the schist, gneisses and quartz-diorite of the Roded Association, and in the Timna Igneous Complex's olivine norite, quartz monzodiorite, and porphyritic granite. Since radiohalos are known to be abundant in similar Precambrian schists, gneisses and granitic rocks (Snelling 2005a), especially the equivalent of the pelitic Elat Schist in the Grand Canyon, it is anticipated that both ^{210}Po and ^{238}U radiohalos would be relatively abundant in these metamorphic and granitic rocks in southern Israel. Their presence could further confirm the catastrophic formation of these granitic rocks, and the catastrophic mode and rate of the regional metamorphism that formed these schists and gneisses (Snelling 1994, 2005a, 2008b).

The pre-Flood/Flood Boundary and the Terminal Precambrian

Austin and Wise (1994) suggested five discontinuity criteria for determining the position of the pre-Flood/Flood boundary in the strata record of any region. These were a mechanical-erosional discontinuity, a time or age discontinuity, a tectonics discontinuity, a sedimentary discontinuity, and a paleontological discontinuity. In applying these criteria to the Grand Canyon-Mojave Desert region of the U.S. Southwest, they identified the boundary as just below the terminal Precambrian Sixtymile Formation just below the Great Unconformity in the Grand Canyon, but within the Neoproterozoic Kingston Peak Formation in the Mojave Desert, with a considerable thickness of terminal Precambrian sedimentary layers above that boundary. In both places there are thick Neoproterozoic sedimentary units sitting on the crystalline basement below this boundary, but in the Grand Canyon the Paleozoic strata sequence immediately overlies the Sixtymile Formation. This is because the terminal Precambrian sedimentary sequence, the earliest deposits of the Flood, thickens westwards from off the higher-standing pre-Flood

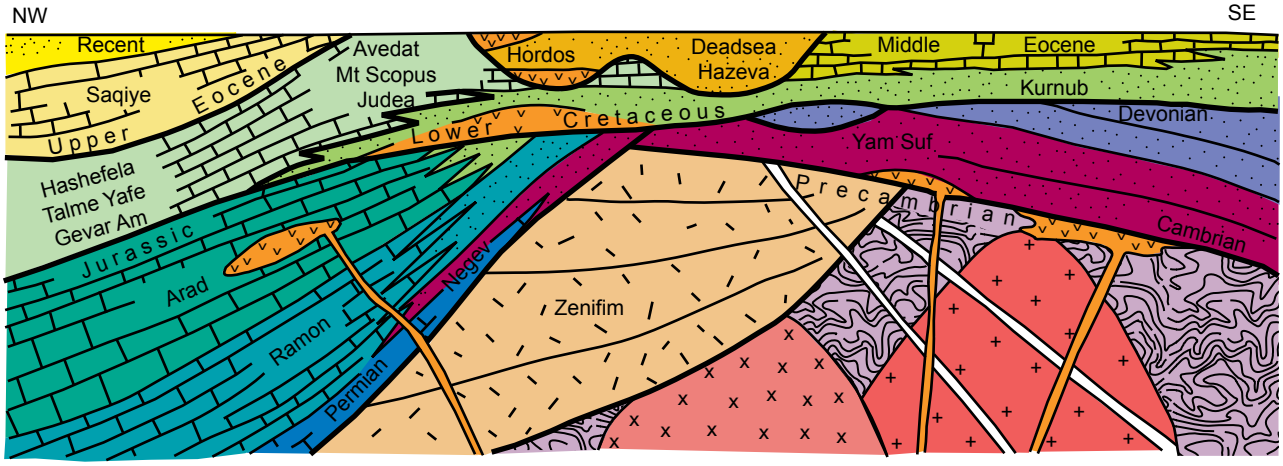

Fig. 11. The generalized stratigraphic sequence across Israel, extending from the Mediterranean coast in the northwest to Arabia in the southeast (after Freund 1977). The relationships between the major rock units of Israel's geology are depicted, with the heavy lines representing the regional unconformities separating six major stratigraphic "packages" of strata. The conventional ages of the tops and bottoms of these strata "packages" are designated. Dotted areas indicate clastic rocks; bricks indicate shales and non-clastic (mainly calcareous) rocks; vs indicate volcanics.

crystalline basement exposed in the Grand Canyon.

A similar situation appears to apply in southern Israel (figs. 3 and 11). In the Elat area the fossiliferous Cambrian sedimentary strata of the early Flood sit directly on the eroded surface of the crystalline basement of the northernmost Arabian-Nubian Shield (Karcz and Key 1966) (figs. 10, 11 and 12), a remnant of the pre-Flood supercontinent that broke apart at the beginning of the Flood (Austin et al. 1994). However, to the north beyond the northern edge of the exposed crystalline basement of the Arabian-Nubian Shield (figs. 11 and 12) the sedimentary strata sequence thickens, and at its base are terminal Precambrian units (Garfunkel 1978). These include unmetamorphosed Neoproterozoic sediments, mainly immature coarse clastics interpreted as molasse-type debris that was deposited on the flanks of the crystalline basement complex as it was eroded and shaped at the end of the Precambrian (Bentor 1961; Picard 1943).

In the Elat region coarse conglomerates (the Elat Conglomerate) interbedded with minor intermediate-rhyolitic volcanics are exposed in small grabens (figs. 4 and 5) that pre-date the erosion of the peneplain surface on the crystalline basement (Bentor 1961; Garfunkel 1978). These sediments consist of coarse, poorly sorted, polymictic conglomerates with a matrix of lithic arkose rich in dark minerals (Garfunkel 1999). The conglomerates are well cemented, with subangular to slightly rounded pebbles and boulders ranging in size from a few centimeters to 1.0 meter (Gutkin and Eyal 1998). Rock units presented as fragments in this conglomerate include all rock units known from the adjacent Precambrian crystalline

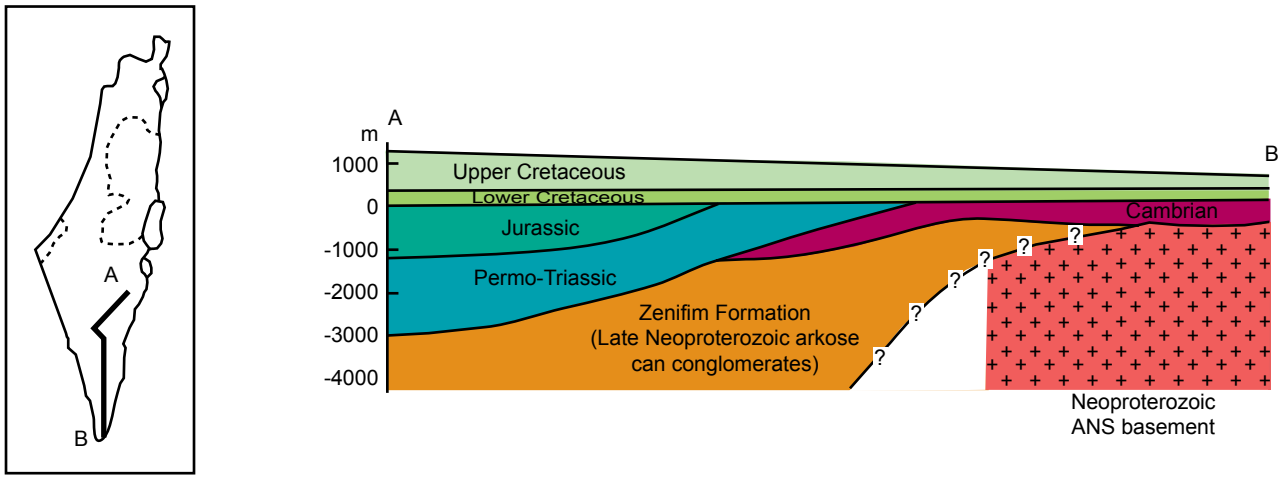

Fig. 12. Schematic stratigraphic cross-section of southern Israel, indicating the major unconformities and the relationships of the terminal Precambrian sediments and the overlying Flood sediments to the Precambrian crystalline basement of the Arabian-Nubian Shield (ANS) (after Veermeesch, Avigad, and McWilliams 2009). The inset map shows the location of this cross-section.

basement. Indeed, the relative amount of pebbles of any rock unit within the conglomerate increases with proximity to the in situ outcrop of this rock unit, which indicates the transport distance during conglomerate deposition must have been very short and therefore deposition was very rapid. Even pebbles derived from the "youngest" andesite and rhyolite dikes on which the conglomerate sits unconformably are one of the main constituents of this Elat Conglomerate (Garfunkel 1999; Gutkin and Eyal 1998). However, a few dikes are intruded into the Elat Conglomerate, indicating both a younger event of dike intrusion post-dating deposition of this conglomerate, and the very short duration of the conglomerate deposition during this continuing sequence of dike intrusions.

Distinct from the Elat Conglomerate, but also unconformably overlying all the eroded crystalline basement rocks including the dikes, is a 200–400 m thick volcano-conglomeratic series that is also preserved in small grabens (Garfunkel 1999) (figs. 4 and 5). This series begins with a basal conglomerate layer similar to that of the Elat Conglomerate, and in the Shelomo area most of its pebbles consist of local quartz-diorite gneiss and migmatite (of the Roded Association) (Gutkin and Eyal 1998). The rest of the series in that area, about 320 m thick, is mainly composed of andesitic-basaltic lavas and pyroclastic flows alternating with several conglomerate layers, and is intruded by hypabyssal andesitic bodies and quartz-porphyry dikes. A few arkose layers are also in this series. Contained boulders are usually big (0.2–1.0 m) and rounded, but comprise only a small percent (2–3%) of the rock's volume.

These exposures of the Elat Conglomerate and the volcano-conglomeratic series probably represent the margins of a large basin known from the subsurface via drilling (Garfunkel 1978), in which the terminal Neoproterozoic Zenifim Formation, more than 2.8 km thick in the Ramon-1 well, accumulated (Garfunkel 1999; Weissbrod 1969) (fig. 11). This formation consists of arkoses, similar to the matrix of the exposed conglomerates, some conglomerates, and small amounts of finer clastics, as well as andesitic volcanics and diabase intrusives, one of which (in the Hameishar-1 well) yielded a K-Ar age of 609±9 Ma (Garfunkel 1999). The available subsurface data from drilling suggests that this terminal Precambrian Zenifim basin which formed north of the Elat area was 150–200 km wide and received the outwash from an uplifted area exposing mainly granitoids and/or gneisses, though some igneous activity also contributed to the basin fill. The source area was probably situated to the south where the northernmost Arabian-Nubian Shield is now exposed in the Elat area and the nearby Sinai, because the grain size of the basin sediments generally tends to decrease northwards.

Applying the five discontinuity criteria of Austin and Wise (1994) to determine the pre-Flood/Flood boundary in southern Israel, there are only two possibilities: the unconformity at the base of the fossiliferous Cambrian strata sequence, or the unconformity between the crystalline basement and the terminal Neoproterozoic coarse clastics with interbedded volcanics (figs. 11 and 12). In any case, these two unconformities merge at the exposed erosion surface on the crystalline basement, which certainly represents a mechanical-erosional discontinuity. There is only a very short time or age discontinuity at both unconformities, and both unconformities represent tectonic discontinuities. So far there is no data on whether the Zenifim Formation contains any fossils, but due to it consisting of coarse immature clastics, the depositional conditions would not have been conducive for fossilization.

Very little data pertaining to the Zenifim Formation is available apart from that obtained in boreholes, so a definitive determination is problematical. However, given some clear similarities between the coarse, poorly sorted, polymictic conglomerates and immature lithic arkoses of the Zenifim Formation (and the Elat Conglomerate and volcano-conglomeratic series) and both the Sixtymile Formation in Grand Canyon and the Kingston Peak Formation in the Mohave Desert, it is considered that on balance the Zenifim Formation (and the related conglomerates) likely represent the initial Flood deposits in southern Israel. With the breaking up of the "fountains of the great deep" triggering the onset of the Flood, massive erosion of the crystalline basement would have occurred, with submarine debris avalanches rapidly accumulating these sediments catastrophically on the flanks of the rifting edges of the pre-Flood supercontinent (Austin et al. 1994; Austin and Wise 1994; Sigler and Wingerden 1998; Wingerden 2003). The presence of interbedded volcanics and contemporaneous explosive volcanism would be testimony to the volcanic activity likely accompanying this breaking up process. Thus the pre-Flood/Flood boundary in southern Israel would be the unconformity between the terminal Proterozoic Zenifim Formation and the erosion surface across the crystalline basement. However, in some places the fossiliferous Cambrian strata sequence sits unconformably directly on that erosion surface across the Precambrian crystalline basement.

Unlike the Grand Canyon-Colorado Plateau area where there is a very large radioisotope time gap between the last igneous activity (the Cardenas Basalt and related diabase sills conventionally regarded as ~1.1 Ga) and the onset of the Flood event near the terminal Precambrian-Cambrian unconformity (Austin 1994; Austin and Wise 1994; Beus and

Morales 2003), in the northernmost Arabian-Nubian Shield area of southern Israel, repeated, almost continuous igneous activity seems to have spanned the last 100 million years or so of the Precambrian right up to, and on into, the onset of the Flood event. The physical manifestation at the earth's surface that the Flood was beginning was the catastrophic "breaking up" of "the fountains of the great deep", but the biblical account doesn't indicate what precursors may have been occurring inside the earth, even for years before, which triggered that "breaking up." From a geophysical perspective, igneous activity had to have built up molten rock and accompanying steam inside the earth under confining pressure until the magma and steam were cataclysmically released by the renting apart of the earth's surface. Thus the rocks resulting from this igneous activity throughout the terminal Precambrian in southern Israel may be the record of this precursor build-up inside the earth that eventually triggered the Flood event. Indeed, the latest igneous activity from about 610Ma onwards has been described as occurring in a crustal extension or rifting tectonic regime, with the intrusion of the Timna alkali granite and monzodiorite followed by the multiple generations of dike swarms, and the initiation of catastrophic erosion and depositional of the Zenifim Formation (Beyth et al. 1994a; Garfunkel 1999).

As for the radioisotope timescale involved, Vardiman et al. (2005) reported five independent evidences that demonstrate a lot of nuclear decay occurred during the Flood event at grossly accelerated rates. A significant biproduct of this accelerated radioisotope decay would have been a huge amount of heat, which would have rapidly increased as the radioisotope decay exponentially accelerated. If this acceleration of radioisotope decay was initiated months before the Flood event began on the earth's surface, then the heat which rapidly accumulated as a result would have begun melting upper mantle and lower crustal rocks. The intrusive igneous rocks produced within those few months would have "aged" radioisotopically by tens of millions of years due to the accelerating nuclear decay, while the pressure confining the molten rock and steam would have built up until they could not be held "in" any longer, so "the fountains of the great deep" were broken up. Such an initiation process would thus explain the close spatial and temporal relationship between the terminal Precambrian igneous activity in the pre-Flood crystalline basement of southern Israel and the tectonic upheaval and catastrophic erosion and deposition which marked the beginning of the cataclysmic Flood event.

Acknowledgments

The logistical support of friends in Israel to accomplish the required field work is gratefully acknowledged. They also assisted in obtaining copies of numerous needed scientific papers, as did my son, Peter. Mark Armitage's help in processing the samples to count the radiohalos is greatly appreciated, as is the financial support of that laboratory work from Ray Strom.

References

Austin, S.A. (ed.). 1994. *Grand Canyon: Monument to catastrophe*. Santee, California: Institute for Creation Research.

Austin, S.A., J.R. Baumgardner, D.R. Humphreys, A.A. Snelling, L. Vardiman, and K.P. Wise. 1994. Catastrophic plate tectonics: A global Flood model of earth history. In *Proceedings of the Third International Conference on Creationism*, ed. R.E. Walsh, pp.609–621. Pittsburgh, Pennsylvania: Creation Science Fellowship.

Austin, S.A., and K.P. Wise. 1994. The pre-Flood/Flood boundary: As defined in Grand Canyon, Arizona and eastern Mojave Desert, California. In *Proceedings of the Third International Conference on Creationism*, ed. R.E. Walsh, pp.37–47. Pittsburgh, Pennsylvania: Creation Science Fellowship.

Bartov, Y., and Y. Arkin. 1980. *Geological photomap*, 1:500,000, 2nd ed. Jerusalem: Geological Survey of Israel.

Baumgardner, J.R. 2003. Catastrophic plate tectonics: The physics behind the Genesis Flood. In *Proceedings of the Fifth International Conference on Creationism*, ed. R.L. Ivey, Jr., pp.113–126. Pittsburgh, Pennsylvania: Creation Science Fellowship.

Be'eri-Shlevin, Y., Y. Katzir, M.J. Whitehouse, and I.C. Kleinhanns. 2009. Contribution of pre-Pan-African crust to formation of the Arabian-Nubian Shield: New secondary ionization mass spectrometry U-Pb and O studies on zircon. *Geology* 37:899–902.

Bentor, Y.G. 1961. Petrographical outline of the Precambrian in Israel. *Bulletin of the Research Council of Israel* 10G:19–63.

Beus, S.S., and M. Morales (eds). 2003. *Grand Canyon geology*, 2nd ed. New York: Oxford University Press.

Beyth, M. 1987. The Precambrian magmatic rocks of Timna Valley, southern Israel. *Precambrian Research* 36:21–38.

Beyth, M., and A. Heimann. 1999. The youngest igneous event in the crystalline basement of the Arabian-Nubian shield, Timna igneous complex. *Israel Journal of Earth Sciences* 48:113–120.

Beyth, M., F.J. Longstaffe, A. Ayalon, and A. Matthews. 1997. Epigenetic alteration of the Precambrian igneous complex at Mount Timna, southern Israel: Oxygen-isotope studies. *Israel Journal of Earth Sciences* 46:1–11.

Beyth, M., and S. Peltz. 1992. Petrology and major-element geochemistry of dikes at Har Timna, southern Israel. *Israel Geological Survey Report GSI/13/92*.

Beyth, M., and T. Reischmann. 1996. The age of the quartz monzodiorite, the youngest plutonic intrusion in the Timna Igneous Complex. *Israel Journal of Earth Sciences* 45: 223–226.

Beyth, M., R.J. Stern, R. Altherr, and A. Kroner. 1994a. The

late Precambrian Timna igneous complex, southern Israel: Evidence for comagmatic-type sanukitoid monzodiorite and alkali granite magma. *Lithos* 31:103–124.

Beyth, M., R.J. Stern, R. Altherr, S. Peltz, and A. Heimann. 1994b. Petrochemistry of dolerite dykes from Mount Timna, southern Israel: Implications for plate tectonic setting. *Geological Survey of Israel Current Research* 9:24–26.

Bielski, M. 1982. On the problem of the Lower Cambrian age in the Arabian-Nubian Massif. In *Numerical dating in stratigraphy*, ed. G.S. Odin, pp. 943–948. Chichester, UK: Wiley.

Buddington, A.F. 1959. Granite emplacement with special reference to North America. *Geological Society of America* Bulletin 70:671–747.

Cohen, B., A. Matthews, M. Bar-Matthews, and A. Ayalon. 2000. Fluid-rock interaction in metamorphosed andesitic dikes, Elat metamorphic complex, Israel. *Israel Journal of Earth Sciences* 49:239–252.

Cosca, M.A., A. Shimron, and R. Caby. 1999. Late Precambrian metamorphism and cooling in the Arabian-Nubian Shield: Petrology and $^{40}Ar/^{39}Ar$ geochronology of metamorphic rocks of the Elat area (southern Israel). *Precambrian Research* 98:107–127.

Eyal, M. 1980. The geological history of the Precambrian metamorphic rocks between Wadi Twaiba and Wadi Um Mara, NE Sinai. *Israel Journal of Earth Sciences* 29:53–66.

Eyal, Y., M. Eyal, and A. Kröner. 1991. Geochronology of the Elat Terrain, metamorphic basement, and its implication for crustal evolution of the NE part of the Arabian-Nubian Shield. *Israel Journal of Earth Sciences* 40:5–16.

Eyal, M., and S. Peltz. 1994. The structure of the Ramat Yotam Caldera, southern Israel: A deeply eroded late Precambrian ash-flow caldera. *Israel Journal of Earth Sciences* 43:81–90.

Freund, R. 1977. Updating the stratigraphic framework of Israel. *Israel Journal of Earth Sciences* 26:30–33.

Friz-Topfer, A. 1991. Geochemical characterization of Pan-African dyke swarms in southern Sinai: From continental margin to intraplate magmatism. *Precambrian Research* 49:477–491.

Ganguly, J. 1972. Staurolite stability and related parageneses: Theory, experiments and applications. *Journal of Petrology* 13: 335–365.

Garfunkel, Z. 1978. The Negev-Regional synthesis of sedimentary basins. In *Sedimentology in Israel, Cyprus, and Turkey*, Tenth International Congress on Sedimentology, Pre-congress Excursion A1, pp. 33–110. Jerusalem: International Association of Sedimentologists.

Garfunkel, Z. 1980. Contribution to the geology of the Precambrian of the Elat area. *Israel Journal of Earth Sciences* 29:25–40.

Garfunkel, Z. 1999. History and paleogeography during the Pan-African orogen to stable platform transition: Reappraisal of the evidence from the Elat area and the northern Arabian-Nubian Shield. *Israel Journal of Earth Sciences* 48:135–157.

Gradstein, F.M., J.G. Ogg, and A.G. Smith. 2004. *A Geologic Timescale 2004*. Cambridge, UK: Cambridge University Press.

Gutkin, V., and Y. Eyal. 1998. Geology and evolution of Precambrian rocks, Mt. Shelomo, Elat area. *Israel Journal of Earth Sciences* 47:1–17.

Halpern, M., and N. Tristan. 1981. Geochronology of the Arabian-Nubian Shield in southern Israel and eastern Sinai. *Journal of Geology* 89:639–648.

Heimann, A., Y. Eyal, M. Eyal, and K.A. Foland. 1995. Thermal events and low temperature alteration in the Precambrian schistose dykes and their host rocks in the Elat area, southern Israel: $^{40}Ar/^{39}Ar$ geochronology. In *Physics and chemistry of dykes*, ed. G. Baer and A. Heimann, pp. 281–292. Rotterdam, Netherlands: A.A. Balkema.

Hutchinson, N.W. 1970. Metamorphic framework and plutonic styles in the Prince Rupert region of the central Coast Mountains, British Columbia. *Canadian Journal of Earth Sciences* 7:376–405.

Ilani, S., A. Flexer, and J. Kronfeld. 1987. Copper mineralization in the sedimentary cover associated with tectonic elements and volcanism in Israel. *Mineralium Deposita* 22:269–277.

Jarrar, G., H. Wachendorf, and G. Saffarini. 1992. A late Proterozoic bimodal volcanic/subvolcanic suite from Wadi Araba, southwest Jordan. *Precambrian Research* 56:51–72.

Jarrar, G., H. Wachendorf, and D. Zachmann. 1993. A Pan-African alkaline pluton intruding the Saramuj Conglomerate, south-west Jordan. *Geologische Rundschau* 82:121–135.

Karcz, I., and C.A. Key. 1966. Note on the pre-Paleozoic morphology of the basement in the Timna area (southern Israel). *Israel Journal of Earth Sciences* 15: 47–56.

Katz, O., D. Avigad, A. Matthews, and A. Heimann. 1998. Precambrian metamorphic evolution of the Arabian-Nubian Shield in the Roded area, southern Israel. *Israel Journal of Earth Sciences* 47:93–110.

Katz, O., M Beyth, N. Miller, P. Stern, D. Avigad, A. Basu, and A. Anbar. 2004. A late Neoproterozoic (~630 Ma) high-magnesium andesite suite from southern Israel: Implications for the consolidation of Gondwanaland. *Earth and Planetary Science Letters* 218:475–490.

Kessel, R., M. Stein, and O. Navon. 1998. Petrogenesis of late Neoproterozoic dikes in the northern Arabian-Nubian Shield: Implications for the origin of A-type granites. *Precambrian Research* 92:195–213.

Kröner, A., M. Eyal, and Y. Eyal. 1990. Early Pan-African evolution of the basement around Elat, Israel, and the Sinai Peninsula revealed by single-zircon evaporation dating, and implications for crustal accretion rates. *Geology* 18:545–548.

Marco, S., H. Ron, A. Matthews, M. Beyth, and O. Navon. 1993. Chemical remanent magnetism related to the Dead Sea Rift: Evidence from Precambrian igneous rocks of Mount Timna, southern Israel. *Journal of Geophysical Research* 98(B9):16,0001–16,012.

Matthews, A., A. Ayalon, A. Ziv, and J. Shaked. 1999. Hydrogen and oxygen isotope studies of alteration in the Timna Igneous Complex. *Israel Journal of Earth Sciences* 48:121–131.

Matthews, A., A.P.S. Reymer, D. Avigad, J. Cochin, and S. Marco. 1989. Pressures and temperatures of Pan-African high-grade metamorphism in the Elat Association, NE Sinai. *Israel Journal of Earth Sciences* 38:1–17.

Picard, L. 1943. Structure and evolution of Palestine with comparative notes on neighboring countries. *Bulletin of the Geology Department, Hebrew University, Jerusalem* 4.

Seck, H.A. 1971. Der einflus des drucks auf die zuzammen-

setzung alkalifeldspathie und plagioclase in system $NaAlSi_3O_8$–$KalSi_3O_8$–$CaAlSi_2O_8$–H_20. *Contributions to Mineralogy and Petrology* 31: 67–86.

Segev, A. 1987. The age of the latest Precambrian volcanism in southern Israel, northeastern Sinai and southwestern Jordan—A re-evaluation. *Precambrian Research* 36:277–285.

Shimron, A.E., and H.J. Zwart. 1970. The occurrence of low pressure metamorphism in the Precambrian of the Middle East and north Africa. *Geologische Mijnbouu* 49:369–374.

Shpitzer, M., M. Beyth, and A. Matthews. 1991. Igneous differentiation in the late Precambrian plutonic rocks of Mt. Timna. *Israel Journal of Earth Sciences* 40:17–27.

Sigler, R., and V. Wingerden. 1998. Submarine flow and slide deposits in the Kingston Peak Formation, Kingston Range, Mojave Desert, California: Evidence for catastrophic initiation of Noah's Flood. In *Proceedings of the Fourth International Conference on Creationism*, ed. R.E. Walsh, pp. 457–501. Pittsburgh, Pennsylvania: Creation Science Fellowship.

Sneh, A., Y. Bartov, T. Wiessbrod, and M. Rosensatt. 1998. *Geological map of Israel*, 1:200,000, 4 sheets. Jerusalem: Geological Survey of Israel.

Snelling, A.A. 1994. Towards a creationist explanation of regional metamorphism. *Creation Ex Nihilo Technical Journal* 8:51–77.

Snelling, A.A. 2000. Geochemical processes in the mantle and crust. In *Radioisotopes and the Age of the Earth: A Young-Earth Creationist Research Initiative*, ed. L. Vardiman, A.A. Snelling, and E. F. Chaffin, pp. 123–304. El Cajon, California: Institute for Creation Research; St. Joseph, Missouri: Creation Research Society.

Snelling, A.A. 2005a. Radiohalos in granites: Evidence for accelerated nuclear decay. In *Radioisotopes and the age of the earth: Results of a young-earth creationist research initiative*, eds. L. Vardiman, A.A. Snelling, and E.F. Chaffin, pp. 101–207. El Cajon, California: Institute for Creation Research, and Chino Valley, Arizona: Creation Research Society.

Snelling, A.A. 2005b. Isochron discordances and the role of inheritance and mixing of radioisotopes in the mantle and crust. In *Radioisotopes and the age of the earth: Results of a young-earth creationist research initiative*, ed. L. Vardiman, A.A. Snelling, and E.F. Chaffin, pp. 393–524. El Cajon, California: Institute for Creation Research, and Chino Valley, Arizona: Creation Research Society.

Snelling, A.A. 2007. Catastrophic granite formation: Rapid melting of source rocks, and rapid magma intrusion and cooling. *Answers Research Journal* 1:11–25.

Snelling, A.A. 2008a. Testing the hydrothermal fluid transport model for polonium radiohalo formation: The Thunderhead Sandstone, Great Smoky Mountains, Tennessee-North Carolina. *Answers Research Journal* 1:53–64.

Snelling, A.A. 2008b. Radiohalos in the Cooma Metamorphic Complex, New South Wales, Australia: The mode and rate of regional metamorphism. In *Proceedings of the Sixth International Conference on Creationism*, ed. A.A. Snelling, pp. 371–387. Pittsburgh, Pennsylvania: Creation Science Fellowship; Dallas, Texas: Institute for Creation Research.

Snelling, A.A. 2008c. Radiohalos in the Shap Granite, Lake District England: Evidence that removes objections to Flood geology. In *Proceedings of the Sixth International Conference on Creationism*, ed. A.A. Snelling, pp. 389–405. Pittsburgh, Pennsylvania: Creation Science Fellowship; Dallas, Texas: Institute for Creation Research.

Snelling, A.A. 2009. *Earth's catastrophic past: Geology, creation and the Flood*. Dallas, Texas: Institute for Creation Research.

Snelling, A.A., and M.H. Armitage. 2003. Radiohalos: A tale of three granitic plutons. In *Proceedings of the Fifth International Conference on Creationism*, ed. R.L. Ivey, Jr., pp. 243–267. Pittsburgh, Pennsylvania: Creation Science Fellowship.

Snelling, A.A., and D. Gates. 2009. Implications of polonium radiohalos in nested plutons of the Tuolumne Intrusive Suite, Yosemite, California. *Answers Research Journal* 2:53–77.

Stacey, J.S., and C.E. Hedge. 1984. Geochronologic and isotopic evidence for early Proterozoic crust in the eastern Arabian Shield. *Geology* 12:310–313.

Stein, M., and S.L. Goldstein. 1996. From plume head to continental lithosphere in the Arabian-Nubian Shield. *Nature* 382:773–778.

Stern, R.A., G.N. Hansen, and S.B. Shirey. 1989. Petrogenesis of mantle-derived, LILE-enriched Archean monzodiorites and trachyandesites (sanukitoids) in southwestern Superior Province. *Canadian Journal of Earth Sciences* 26:1688–1712.

Stern, R.J., and W.I. Manton. 1987. Age of Feiran basement rocks, Sinai: Implications for the late Precambrian crustal evolution in the northern Arabian-Nubian Shield. *Journal of Geological Society of London* 144:569–575.

Sultan, M., K.R. Chamberlain, S.A. Bowring, R.E. Arvidson, H.T. Abuzied, and B. El Kaliouby. 1990. Geochronologic and isotopic evidence for involvement of pre-Pan-African crust in the Nubian shield, Egypt. *Geology* 18:761–764.

Vardiman, L., A.A. Snelling, and E.F. Chaffin (eds). 2005. *Radioisotopes and the age of the earth; Results of a young-earth creationist research initiative*. El Cajon, California: Institute for Creation Research, and Chino Valley, Arizona: Creation Research Society.

Vermeesch, P., D. Avigad, and M.O. McWilliams. 2009. 500 m.y. of thermal history elucidated by multi-method detrital thermochronology of north Gondwana Cambrian sandstone (Eilat area, Israel). *Geological Society of America Bulletin* 121:1204–1216.

Weissbrod, T. 1969. The Paleozoic of Israel and adjacent countries: The Paleozoic stratigraphy of southern Israel. *Geological Survey of Israel Bulletin* 47.

Wingerden, V. 2003. Initial Flood deposits of the western North American Cordillera, California, Utah and Idaho. In *Proceedings of the Fifth International Conference on Creationism*, ed. R.L. Ivey, Jr., pp. 349–358. Pittsburgh, Pennsylvania: Creation Science Fellowship.

Winkler, H.G.F. 1979. *Petrogenesis of metamorphic rocks*, 5th ed. Berlin:Springer-Verlag.

Wyllie, P.J., W.-L. Huang, C.R. Stern, and S. Maaloe. 1976. Granitic magmas: Possible and impossible sources, water contents, and crystallization sequences. *Canadian Journal of Earth Sciences* 13:1007–1019.